JOURNAL OF GEOPHYSICAL RESEARCH, VOL. 105, NO. B5, PAGES 11,001-11,019, MAY 10, 2000

Time-resolved study of charge generation and propagation in igneous rocks

Friedemann Freund

SETI Institute and Department of Physics, San Jose State University, San Jose, California
NASA Ames Center, Moffett Field, California

Abstract. Electrical resistivity changes, ground potentials, electromagnetic (EM), and luminous signals preceding or accompanying earthquakes have been reported many times, in addition to ground uplift and tilt and other parameters. However, no concept exists that would tie these diverse phenomena together into a physically coherent model. Using low- to medium-velocity impacts to measure electrical signals with microsecond time resolution, it is observed that when gabbro and diorite cores are impacted at relatively low velocities, ≈100 m/s, highly mobile charge carriers are generated in a small volume near the impact point. They spread through the rocks, causing electric potentials exceeding +400 mV, EM, and light emission. As the charge cloud spreads, the rock becomes momentarily conductive. When a granite block is impacted at higher velocity, ≈1.5 km/s, the propagation of the *P* and *S* waves is registered through the transient piezoelectric response of quartz. After the sound waves have passed, the surface of the granite block becomes positively charged, suggesting the same charge carriers as observed during the low-velocity impact experiments, expanding from within the bulk. During the next 2-3 ms the surface potential oscillates, indicating pulses of electrons injected from ground and contact electrodes. The observations are consistent with positive holes, e.g., defect electrons in the O^{2-} sublattice, traveling via the O 2p-dominated valence band of the silicate minerals. The positive holes propagate as charge clouds rather than as classical EM waves. Before activation, they lay dormant in form of electrically inactive positive hole pairs, PHP, chemically equivalent to peroxy links, $O_3X/^{OO}\backslash XO_3$ with $X=Si^{4+}$, Al^{3+}, etc. PHPs are introduced into the minerals by way of hydroxyl, O_3X-OH, which all nominally anhydrous minerals incorporate when crystallizing in H_2O-laden environments. The fact that positive holes can be activated by low-energy impacts, and their attendant sound waves, suggests that they can also be activated in the crust by microfractures during the dilatancy phase. Depending on where in the stressed rock volume the charge carriers are activated, they will form rapidly moving or fluctuating charge clouds that can account for earthquake-related electrical signals and EM emission. Wherever such charge clouds intersect the surface, high fields are expected, causing electric discharges and earthquake lights.

1. Introduction

Seismic waves are the most obvious manifestation of earthquakes. However, earthquakes may also be accompanied or preceded by signals of a different nature (electric, electromagnetic, and luminous) that may help forecasting impending seismic activity. Earthquake research has struggled for decades to decipher them. A broadly held view [*Bolt*, 1988; *Eiby*, 1980; *Meyer*, 1977; *Rikitake*, 1976] is that the development of an earthquake-prone region can be divided into the five evolutionary stages depicted schematically in Figure 1.

Stage 1 is buildup of elastic strain. As two sides of a fault move, the rocks become compressed.

Stage 2 is dilatancy. After the rocks are compressed as tightly as possible, the only way for them to change shape is to buckle and expand. A key notion is the formation of microcracks. The increase in volume leads to uplift and tilting, while the decrease in electrical resistivity is believed to be caused by water and brine, forced out from pores and forming interconnected films.

Paper number 1999JB900423.
0148-0227/00/1999JB900423$09.00

Stage 3 is thought to be marked by influx of water or brine back into microcracks and pores, causing the rocks to loose their previously acquired strength, while continuing to experience a decrease in electrical resistivity.

Stage 4 is marked by sudden fault rupture when the rocks can no longer withstand the accumulated strain, releasing the accumulated energy and producing an earthquake.

Stage 5 contains the aftershocks that are triggered by the sudden strain release in the hypocenter and continue until stable conditions return throughout the affected rock volume.

This "standard model", as it may be called, is based on a relatively simple physical concept, namely, (1) that brines are generally present throughout the crust and (2) that they are forced out of previously closed pores during the dilatancy stage 2 but flow back during the influx stage 3, thereby causing the described changes in seismic *P* velocity, rock volume, radon release, and electrical resistivity.

The model depends upon the amount of water or brine that is available in the crust throughout the seismogenic depth range. *Wannamaker* [1994, 2000] argues that highly saline fluids may widely occur in fractured horizons as observed in crystalline basement rocks penetrated by drilling [*Fritz and Frape*, 1987], making it possible for the conductivity of the rocks to be enhanced by much smaller amounts of fluid than

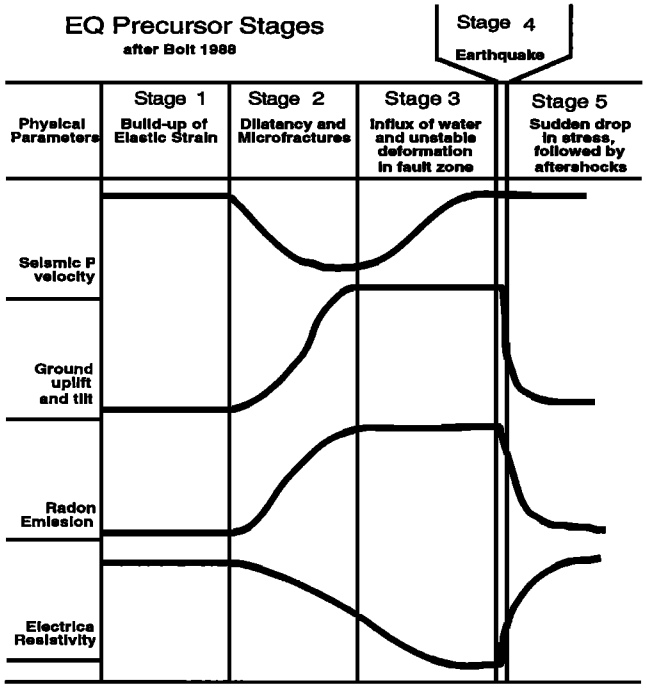

Figure 1. Earthquake precursor stages as proposed by *Bolt* [1988] to link seismic, geodesic, radon emission, and electrical resistivity observations.

hitherto thought necessary. *Yardley and Valley* [2000] point out that such a scenario is limited to cold rocks and that drilling had to be abandoned in the deepest hole because of loss of drill fluid into the surrounding rocks [*Borevsky et al.*, 1995]. This is consistent with the suggestion that the partial pressure of fluid species in any interconnected grain boundary network in the deeper and therefore hotter crust will generally be buffered by the mineral equilibria [*Yardley and Valley*, 1997]. The reason is that in rocks cooled from an original equilibration temperature at least 50-100°C higher than the temperature today, retrograde reactions of minerals formed under peak conditions will result in a lowering of fluid partial pressures, leading to the absence of a free fluid phase, except in isolated fluid inclusions [*Frost and Bucher*, 1994; *Valley et al.*, 1990]. It is also worth noting that if fluid-filled fractures were a major source of crustal conductivity, the conductivity should be highest at shallow depths where open cracks are most abundant [*Yardley and Valley*, 2000]. This is generally not observed.

Another agent for enhancing the electrical conductivity could be graphite such as found during deep drilling projects in graphite-rich zones exhibiting exceptionally high conductivities [*ELEKTB Group*, 1997; *Emmermann and Lauterjung*, 1997]. However, graphite films are not universal in the lower crust [*Yardley and Valley*, 1997], though *Frost et al.* [1989] have presented arguments for thin carbon films deposited while free fluids were present in the rocks.

While the "brines out and brines in" concept may reaonably well explain the slow, quasi-continuous electrical resistivity changes of the rock volume as depicted in Figure 1, it does not provide a physical basis for the other more enigmatic signals such as electromagnetic emission and earthquake lights that require rapidly moving charges and high electric fields, respectively. Progress can be expected if we find a physical process that can account for all types of signals, including those that are not covered by the standard model.

1.1. Precursor Signals

In geophysical settings, stress and strain are usually looked at as long-range phenomena, accumulating over many kilometers. In absolute terms, the stress changes during a seismic event are not very large, <3 MPa at the hypocenter and <1 MPa in the nearfield, that is, within one rupture dimension as discussed in the context of the 1992 *M*7.3 Landers earthquake [*Landers*, 1994]. During the period leading up to an earthquake the stress changes are even smaller, ~3 orders of magnitude smaller, i.e., in the kilopascal range. However, it is to be acknowledged that signals emitted from a large rock volume under stress may have their origin in many small events that take place on the scale of individual mineral grains. Though the overall stress change may be low, stresses tend to concentrate locally. As a result, mineral grains slip along their boundaries, deform through bursts of mobilized dislocations, or initiate microfractures that open explosively and close. These microscale events punctuate the average stress change. Occurring deep in the crust, their signals cannot be resolved individually, but their accumulative effect may become detectable from afar.

While there seems to be a growing feeling that at least some earthquake precursor signals other than those listed in Figure 1 are plausible [*Bernard*, 1992; *Johnston*, 1997], the standard model fails to merge the diverse contributions into a physically coherent theory. This is nowhere more apparent than for those signals that require, as their underlying physical cause, the generation of electric charges that are free to propagate in the rock volume [*Dobrovolsky et al.*, 1989; *Park*, 1997a]. Such charges and the signals as they may emit are in part quite controversial [*Geller*, 1997; *Michael*, 1996; *Pham et al.*, 1998]. In some cases such as at Parkfield, California, where the electrical conductivity along and across the San Andreas fault system has been monitored for over 10 years [*Park*, 1997b], no clear changes in the conductivity or any other electric effects related to seismicity have been identified [*Park*, 1998].

Broadly speaking, electric and electromagnetic (EM) signals can be divided into three categories: (1) ground potentials and EM emission, (2) luminous phenomena, and (3) perturbations in the ionosphere.

1. Ground potentials can be generated as "streaming potentials" when brines, moving through porous rocks, entrain ionic charges [*Bernabé*, 1998; *Draganov et al.*, 1991; *Morrison et al.*, 1989; *Stesky*, 1986]. Another way of producing ground potential is through stress applied to rocks containing piezoelectric minerals such as quartz [*Bishop*, 1981; *Finkelstein et al.*, 1973; *Morat and LeMouel*, 1987, 1992], maybe also in the absence of piezoelectric minerals [*Varotsos et al.*, 1997]. The transmission of stress over large distances to explain mV signals recorded in Greece has been hotly debated [*Geller*, 1996; *Huang and Ikeya*, 1998; *Masood*, 1995]. Low-frequency EM emissions from the ground are less controversial, as was recently stated in reviews by *Parrot and Johnston* [1989], *Park et al.* [1993], and *Johnston* [1997]. Low-frequency EM emissions have been documented by the Stanford group [*Fraser-Smith*, 1992; *Fraser-Smith et al.*, 1990] in connection with the 1989 Loma Prieta earthquake in California. The origin of these signals and how they are

transmitted over long distances are unknown [*Bernard*, 1992]. *Merzer and Klemperer* [1997] successfully modeled the signals emitted prior to the Loma Prieta earthquake by assuming a thin, highly conductive layer along the fault that magnified the external EM waves incident on the Earth's surface. Likewise EM emission was recorded during the 1989 Ito seismic swarm in Japan [*Fujinawa and Takahashi*, 1990]. Detection of EM signals is pursued by groups in Japan, China, and countries of the former Soviet Union [*Fujinawa and Takahashi*, 1993; *Molchanov et al.*, 1992; *Serebryakova et al.*, 1992; *Zhijia*, 1989].

2. Particularly puzzling, in part intertwined with folklore as reviewed by *Tributsch* [1983], are luminous phenomena reported to accompany some large earthquakes [*Derr*, 1973; *Hedervari and Noszticzius*, 1985], occasionally also weak events such as in 1988 in the Saint John region of Canada [*Quellet*, 1990]. Striking examples are the earthquake lights during the 1966 earthquake at Matsushiro, Japan, that illuminated the hilltops for 96 s and were photographed by T. Kuribayashi [see, e.g., *Derr*, 1986]. Such luminous phenomena may be caused by piezoelectricity from quartz-bearing rocks [*Finkelstein et al.*, 1973] or by sonoluminescence [*Johnston*, 1991], but they cannot be integrated into a fluid-driven dilatancy model [*Nur*, 1974].

3. Ionospheric perturbations over earthquake regions have been noted during the 1964 Alaskan earthquake [*Davis and Baker*, 1965] and in regions outside the contiguous United States [*Bilichenko et al.*, 1990; *Chmyrev et al.*, 1986; *Drobzhev et al.*, 1978; *Galperin et al.*, 1985; *Gokhberg et al.*, 1988; *Larkina et al.*, 1988; *Molchanov and Hayakawa*, 1998a,b; *Parrot and Johnston*, 1989] such as over Kobe a few days before and after the January 1995 earthquake [*Molchanov et al.*, 1998], though no electromagnetic ground signals were observed during the aftershocks [*Yoshida et al.*, 1995].

1.2. Known Sources of Electric Charges in Rocks

Principal sources for the generation of electric charges are "streaming potentials," "piezoelectricity," "triboelectricity" and "triboluminescence," and "contact electrification."

Streaming potentials agree best with the "brines-out and brines-in" concept. They can occur in fluid-saturated rocks when, under the influence of external stress, fluids move through an interconnected pore space. If the fluids entrain solvated ions of one sign, while the charge-balancing counterions stay adsorbed to the rocks, electric potentials can, in principle, be generated over relatively large distances [*Bernabé*, 1998; *Draganov et al.*, 1991; *Morrison et al.*, 1989; *Stesky*, 1986]. In natural rocks the streaming potentials are limited in magnitude by the conductivity of the brines, while in technical situations such as in oils pumped as coolants through transformers, the accumulation of charges can lead to dangerously high electric fields [*Oommen*, 1988].

Piezoelectricity describes the phenomenon that, when a stress is applied to certain crystals in certain crystallographic directions, opposite sides of the crystals become oppositely charged due to subtle displacements of the ions in the structure [*Finkelstein et al.*, 1973]. Piezovoltages occur in crystals that belong to a symmetry class with polar axes, that is, without inversion center and axes perpendicular to mirror planes. The voltages disappear instantly when the stress is removed. Furthermore, because piezopotentials are of opposite sign on opposing faces of each individual crystal, they cancel within a stressed rock containing piezoelectric crystals in random orientation. (While this is strictly true for the volume, for instance for a granite solidified in a stress-free setting, at the surface of a block removed from a larger volume the symmetry is broken, allowing piezopotentials to appear [*Nitsan*, 1977].)

Triboelectricity and triboluminescence describe phenomena that when crystals are violently rubbed, abraded, indented or fractured, sparks may be observed. On an atomic level, many different processes contribute to these effects ranging from the generation and rapid movement of dislocations (thereby creating exciton pairs, i.e., electrons and holes, which give off light upon recombination) to high local charges developing across rapidly advancing fracture wedges. The resulting high fields lead to discharges across the opening gap, to local, short-circuited current, to neutral and electronically excited atom emission, and to visible light [*Dickinson et al.*, 1986; *Enomoto and Hashimoto*, 1990]. Triboelectricity manifests itself during deformation, indentation or fracture [*Hadjicontis and Mavromatou*, 1994; *Yoshida et al.*, 1997, 1998] or the explosive disintegration of rocks upon compressive loading as reported by *Brady and Rowell* [1986].

Contact electrification occurs whenever two different nonconductive materials are brought in contact. It arises because even insulators have a nonzero density of free charge carriers, either electrons or holes or both. These charge carriers define a Fermi level similar to the Fermi level in metals and semiconductors [*Kittel*, 1980]. Upon touching, charges flow from one insulator to the other until the Fermi levels are equalized across the contact. An exemplary experiment describing charge transfer between mica and quartz has been reported by *Horn and Smith* [1992]. While potentially important in technical applications, contact electrification plays no role in in situ rock electrodynamics.

None of the mechanisms listed stands out as a candidate for merging the electrical, electromagnetic and luminous phenomena reportedly associated with earthquakes into a single, coherent physical model. There are only two ways out of this dilemma. Either we accept the premise of the standard model with its simple brine-out and brine-in concept, leaving no room for any "exotic" electrical and luminous phenomena allegedly associated with earthquakes, or we consider the possibility that in spite of decades of intense studies in many laboratories worldwide, rocks may contain charge carriers that have not yet been identified.

1.3. Less Well-Known Sources of Electric Charges in Rocks

Basically, there are only two kinds of charges that can carry electric current: ions and electrons.

Ionic charge carriers dominate the high-temperature regime of the electrical conductivity of rocks where melting or partial melting occurs [see, e.g., *Kariya and Shankland*, 1983]. Electrolytic conductivity, for example currents transported by solvated ions in aqueous solution (e.g., in brines), falls into the same category, extending the range of ionic conductivity downward in temperature.

Electronic charge carriers, prevalent in metals and semiconductors, are thought to be of lesser concern in rocks because rocks are mostly good insulators. Electronic charge carriers are either electrons or defect electrons, the latter also known as "holes." In minerals, electrons and holes can be associated with cations that change from one oxidation state to another such as the redox pair Fe^{2+}/Fe^{3+}. If minerals contain local structural environments that allow for an exchange of electrons among neighboring transition metal cations, hole

conductivity can take place. However, except for special cases where Fe^{2+} and Fe^{3+} exist in high concentrations and on crystallographically well-defined sites such as in spinels, foremost magnetite [*Dieckmann et al.*, 1983], electron exchange by this mechanism is very limited. Even in Fe-rich silicates such as some pyroxenes, amphiboles, or olivine [*Schock and Duba*, 1985; *Shankland*, 1981], electronic conduction via the cation sublattice is negligible at low to moderate temperatures [*Shankland and Ander*, 1983].

What is generally not acknowledged is the fact that oxygen can also exist in two oxidation states: as O^{2-} in the common 2- oxidation state and as O^- in the somewhat uncommon 1- oxidation state. Because mineral structures in textbooks and elsewhere are invariably formulated with the tacit assumption that oxygen is never anything else but O^{2-}, few in the geosciences are aware that oxygen is not locked into its 2- oxidation state and that, given the right conditions, an O^- in an O^{2-} matrix represents a powerful electronic charge carrier. An O^- in an O^{2-} matrix is a hole, but different from holes residing on the cation sublattice. To make the distinction clear, an O^- in an O^{2-} matrix is called a "positive hole" [*Griscom*, 1990].

The O^- has a dual character, a fact that can give rise to some confusion. From a chemist's perspective, an O^- is an oxygen anion with an incomplete valence shell, 7 electrons instead of 8. It is a radical, and writing it as O• is equally justified. If the O^- is part of an XO_4^{4+} complex (X = Si^{4+}, Al^{3+}, etc.) the structural building block of all common silicate minerals, it might be written either as XO_4^{3+} or as $O_3X/^{O\bullet}$ [*Marfunin*, 1979]. Being radicals, $O^- \equiv O\bullet$ and $XO_4^{3+} \equiv O_3X/^{O\bullet}$ are reactive. They can react with transition metal cations, causing their oxidation, e.g. $Fe^{2+} + O^- = Fe^{3+} + O^{2-}$ or $Fe^{2+} + XO_4^{3+} = Fe^{3+} + XO_4^{4+}$. They can self-trap by pairing up with another O^- to form a positive hole pair, PHP, chemically equivalent to a peroxy anion, $O^- + O^- = O_2^{2-}$ or a peroxy link $O_3X/^{O\bullet} + {}_{\bullet}O/XO_3 = O_3X/^{OO}\backslash XO_3$. Note that the O^-–O^- distance in the peroxy bond is ~1.5 Å [*Cremer*, 1983], only about half the value for O^{2-} ...O^{2-} distances in most mineral structures, 2.8-3.0 Å. The shortness of the O^-–O^- bond implies a small partial molar volume of the peroxy-bound oxygen.

From a physicist's perspective, the O• or $O_3X/^{O\bullet}$ represents an electronic defect, namely a defect electron or positive hole as defined above. A peroxy anion or peroxy link, O_2^{2-} or $O_3X/^{OO}\backslash XO_3$, then represent a self-trapped positive hole pair, PHP [*King and Freund*, 1984; *Freund et al.*, 1994]. The PHP is the spin-coupled, electrically inactive state in which positive holes will normally be found in the various minerals. If the coupling is weak, the PHP may dissociate, releasing a positive hole.

Adopting the band model, a positive hole can be described as a partially filled state near the upper edge of the valence band that has strong O 2p character. The valence band is separated from the conduction band by a wide energy gap. With all levels filled, no electrons can flow causing conductivity. If one O^{2-} in the O^{2-} matrix changes to O^-, creating a positive hole, electrons from neighboring O^{2-} can transition onto the O^- site. In this way the positive hole becomes mobile. It turns into an electronic charge carrier that hops from O^{2-} to O^{2-} site. The hopping frequency is controlled by the thermal phonons, for example by the frequency of collisions between neighboring O^{2-}, typically 10^{12} s^{-1}, as an enabling process to transfer an electron from an O^{2-} onto an O^- [*Shluger et al.*, 1992; *Deb and Chandorkar*, 1995]. Multiplying the phonon frequency with the hopping distance, ~3 Å, and a probability factor of 1/3 that the hopping occurs in the right direction, the maximum speed with which a positive hole could propagate can be estimated to fall into the range of 100-300 m/s.

To further understand why positive holes are of interest in the context of earthquake-related electrical phenomena, we need to address the question of how the PHPs form in mineral structures in the first place. It had been noted early [*Martens et al.*, 1976] that OH^-, introduced into the structure of nominally anhydrous MgO through dissolution of small amounts of H_2O at the time of crystallization in an H_2O-laden environment, can undergo a previously unknown redox conversion. This reaction involves two OH^- at Mg^{2+} vacancies, compensating for the missing cation charges:

$$(H_2O)_{dissolved} + (O^{2-})_{structure} \Leftrightarrow (OH^-)_{structure} + (OH^-)_{structure}. \quad (1)$$

These two OH^- at a cation vacancy site split off molecular H_2 while oxidizing two O^{2-} to O^- which undergo self-trapping to a peroxy anion, O_2^{2-}, e.g., a PHP:

$$(OH^-)_{structure} + (OH^-)_{structure} = (H_2)_{structure} + (O_2^{2-})_{structure}. \quad (2)$$

The presence of H_2 molecules in the MgO matrix was confirmed spectroscopically [*Freund and Wengeler*, 1982]. Evidence for the presence of the PHPs was obtained by measuring the electrical conductivity, magnetic susceptibility, dielectric polarization and other physical properties that are affected by the dissociation of PHP and generation of positive holes [*Freund et al.*, 1993, 1994; *Kathrein and Freund*, 1983]. The behavior of positive holes as mobile charge carriers was treated in the context of classical semiconductor theory [*King and Freund*, 1984].

If this OH^- redox conversion occurs in MgO, the question arose whether an analogous redox conversion would take place in nominally anhydrous silicate minerals that invariably contain traces of H_2O after crystallizing in H_2O-laden magmatic or metamorphic environments, forming O_3X–OH [*Bell and Rossman*, 1992; *Rossman*, 1996; *Smyth et al.*, 1991]:

$$(H_2O)_{dissolved} + (O_3X/^{O}\backslash XO_3)_{structure} \Leftrightarrow (O_3X/^{OH}{}_{HO}/XO_3)_{structure} \quad (3)$$

The redox conversion would involve O_3X-OH pairs and cause them to exchange electrons in such a way as to reduce their two H^+ to H_2 and oxidize their two O^{2-} to O^-. These O^- would in turn undergo spin-pairing and tie a peroxy link:

$$(O_3X/^{OH}{}_{HO}/XO_3)_{structure} = (H_2)_{structure} + (O_3X/^{OO}\backslash XO_3)_{structure}. \quad (4)$$

Peroxy links in fused SiO_2 were studied theoretically by *Edwards and Fowler* [1982] and experimentally by electron spin resonance spectroscopy [*Friebele et al.*, 1979] and dielectric polarization [*Freund and Masuda*, 1991]. Even minerals from highly reducing crustal and upper mantle environments such as olivine probably contain peroxy links, introduced via the dissolution of small amount H_2O [*Freund and Oberheuser*, 1986]. Further information about PHPs in olivine was obtained through dielectric polarization measurements (F. Freund, unpublished results, 1998) and single crystal fracture experiments [*Freund and Ho*, 1996].

It is well known that the O^-–O^- bond is not strong, in spite of its shortness (~1.5 Å compared to typical O^{2-}–O^{2-} distances of 2.8-3.0 Å [*Cremer*, 1983]). It can break by reorienting

toward a different oxygen partner. This process involves O diffusion [*Edwards and Fowler*, 1982; *Hamann*, 1998]. Alternatively, the O^-–O^- bond can dissociate in the way described above, releasing a positive hole. This process does not involve O diffusion but only the generation of electronic charges. Continuing from (2) and (4) we have

$$(O_2^{2-})_{structure} = (O^- + O^-)_{structure} \quad (5)$$

$$(O_3X/^{OO}\backslash XO_3)_{structure} = (O_3X/^{O^\bullet}{}_{\bullet O}/XO_3)_{structure}. \quad (6)$$

A last point to mention concerns the p-type conductivity that results from the mobilization of the positive holes according to (5) and (6). The only as mobile charge carriers generated by the PHP dissociation are positive holes. No mobile negative charges are generated at the same time.

This is best understood if we look at a predominantly ionic mineral structure such as MgO where the PHPs are associated with Mg^{2+} vacancies [*Freund et al.*, 1993]. The two holes trapped at the oxygen sites (two positive charges relative to O^{2-}) fully compensate the charge of the cation vacancy (two negative charges relative to Mg^{2+} occupying the cation site). When the PHP dissociates and one positive hole propagates outward, the Mg^{2+} vacancy is left behind with one remaining positive hole. This half-compensated Mg^{2+} vacancy is a single negative charge. Its mobility is nil because Mg^{2+} cations only diffuse at high temperatures, >700°C [*Wuensch et al.*, 1973; *Sempolinski and Kingery*, 1980]. Similar analogous arguments can be made for PHP in predominantly covalent structures such as SiO_2 or feldspars, where the XO_4 are linked at all four corners by O_3X–O–XO_3 bonds. After $O_3X/^{OO}\backslash XO_3$ dissociation according to equation (6) one XO_4^{4+} and one XO_4^{3+} remain [*Marfunin*, 1979]. This configuration represents a negative charge that is stationary compared to the high mobility of the positive hole.

When a situation arises as described here that the only mobile charge carriers are positive holes, electrostatic interaction between these holes causes the charge carriers to repel each other and to diffuse toward the surface. This outward flow of positive holes continues until the mutual repulsion between the charge carriers is balanced by the electric field between the surface and the bulk [*King and Freund*, 1984]. This leads to two predictions: (1) The positive surface potential at the surface is a function of the dielectric contrast between the solid and the surrounding medium, say vacuum or air, $\varepsilon \sim 1$. For a material with a dielectric constant of $\varepsilon \sim 10$ the calculated potential at the flat surface is +420 mV. (2) The thickness of the subsurface charge layer and hence the magnitude of the electric field are a function of the concentration of mobile positive holes. When the hole concentration increases from 10 ppm to 100 ppm (10^{17} to 10^{18} cm^{-3}), the field increases from 1.2×10^5 to 4×10^5 V/cm, high enough to consider dielectric breakdown of the surrounding air.

This raises the question whether some of the exotic electrical and electromagnetic signals reportedly associated with earthquakes could be caused by positive hole-type charge carriers. To answer this question, we have to experimentally test whether or not common igneous rocks generate positive hole charge carriers, and if so, how and under which conditions.

1.4. Why Impact Experiments?

The idea to conduct impact experiments came from fracture experiments with MgO crystals [*Dickinson et al.*, 1986] which suggested that the acoustic waves emitted during brittle fracture are capable of dissociating the PHPs in the MgO matrix according to equation (5), thus activating positive hole charge carriers. An impact creates similar effects as microfractures that open and close explosively: It generates bursts of mobile dislocations and acoustic waves that propagate through the rock. Fracture experiments with olivine crystals also suggested that under the effect of the acoustic waves emitted during brittle fracture, positive holes were activated according to equation (6).

As mentioned in section 1.1, stress accumulation in a large rock volume prior to an earthquake is expected to lead to events in microvolumes, on the scale of mineral grains, that resemble events caused by an impact experiment. In the field, in an earthquake-prone region, such microevents are distributed over time and space. During impact experiments, however, we can simulate them with microsecond timing, far better than by conventional rock fracture experiments [*Brady and Rowell*, 1986; *Cress et al.*, 1987; *Hadjicontis and Mavromatou*, 1994]. During a low-velocity impact the sudden stress will be concentrated in a small volume near the impact point that may become the source volume for positive hole charge carriers. During medium-velocity impacts the acoustic waves become more energetic, possibly carrying enough punch to activate PHPs and to generate positive holes in their wake.

2. Experimental Procedures

2.1. Low-Velocity Impact Experiments

Low-velocity impact experiments were conducted using a compound crossbow with a span of close to 1 m, screwed to a 2-cm-thick Al metal base that rested on vibration-isolation pads and was additionally weighed down with 50-kg lead ingots [*Freund and Borucki*, 1999]. The crossbow launched a Teflon sabot carrying the stainless steel, 1/8-inch to 1/4-inch (3.1-6.3 mm) diameter projectiles to a terminal velocity close to 100 m/s, determined by a series of photodetectors in the flight path. As the sabot hit a stop, the projectiles passed through an Al foil to strip electrostatic charges and continued in free flight for 50 mm before impacting the sample. The kinetic energy carried by the impactors ranged from 0.06 J for 1/8-inch to 0.43 J for 1/4-inch steel balls. The samples were cylindrical rock cores, 3/4-inch (20 mm) diameter, up to 4-inch (100 mm) long, as obtained with a diamond drill. Their faces were polished. The air-dry cores were mounted in a nylon block, firmly attached to the base. A metal screw through the nylon block, in contact with the rock samples, served as a grounding point. Shots with the small projectiles left small whitish marks on the front face of the rock cores. Repetitive shots with medium to larger projectiles led to chipping and fracture.

A variety of sensors were applied to the rock cores: (1) axially mounted magnetic pick-up coils (2 cm wide, 3000 turns, 30 gauge magnetic wire), (2) photodiodes (Centronix OSY 5V-10M/10K with integrated op amplifiers), placed either near the front at a distance of 20-30 mm from the rock, angled at ~45° so as to "see" the entire front face, or at the far end at 10 mm from the rock with tubes to restrict the field of view to the rim or the flat face, (3) a ring capacitor near the front made of Al tape, 7 mm wide, insulated from the rock by a 250-μm-thick sheet of polyethylene, (4) a plate capacitor at the back end made of Al sheet, 20 mm diameter, with 250-μm poly-

ethylene insulation, and (5) up to three ring electrodes made of 4-mm-wide adhesive Cu tape, attached directly onto the rock surface. Currents flowing from the electrodes into the rocks were measured through the voltage drop across a 2.4-MΩ resistance to ground. Positive voltages indicate electrons flowing toward the rock. The grounding point was about 2/3 down the length of the cores, measured from the front face. The front photodiodes were occasionally destroyed by ricocheting steel balls. For data acquisition we used a 200 MHz digital 4-Channel Tektronix oscilloscope, model TDS 420A. The data were acquired from the trigger point minus 5 ms onward until the buffer was full, typically after ~30 ms.

2.2. Medium-Velocity Impact Experiments

The medium-velocity impact experiments were conducted in the NASA Ames Vertical Gun Range (AVGR) with 1/4-inch (6.3 mm) diameter Al spheres as impactors, using the powder gun stage of the AVGR at vertical incidence in a vacuum of 2-4 mbar. To strip the Al impactors of adventitious electrostatic charges which they might have accumulated during acceleration, upon leaving the gun barrel, they pierced through a grounded thin Al foil.

The 25 x 25 x 20 cm block of rock was instrumented with three types of sensors:

1. Three magnetic pick-up coils on 26 x 26 cm square wooden frames with 300 windings of 30 gauge magnet wire. One of these coils was positioned 10 cm above the plane of impact to record primarily the emission from the plasma plume [*Crawford and Schultz*, 1988, 1991]. The two other coils were positioned slightly below midheight and near the bottom of the block, respectively. The response of the coils is a function of their resonant frequencies as well as the shape of the input signal. Though the spacing between the coils was less than their diameters, the self-induction of the coils was found to be negligible.

2. Three capacitor stripes, 22 cm long, 20 mm wide, consisted of pieces of 0.05-mm-thick electrical insulation tape glued to the rock surface and backed by 20-cm-long, 12-mm-wide adhesive Cu tape. The capacitor sensors were all on one side of the block, one near the top (e.g. in the plane of impact), another one at midheight, and the third one near the bottom. The voltage registered by the capacitive sensors is called "positive" when the rock surface became positively charged.

3. Two strips of adhesive conductive Cu tape, 20 cm long, 12 mm wide, were glued directly onto the rock surface, thus providing direct metal-to-insulator contacts. Both electrodes were placed on the side of the block opposite to the capacitive sensors: one was in the plane of impact, the other one near the bottom. Both electrodes were connected to ground through 2.4-MΩ resistances across which the voltage drop was measured. The voltage is called positive when the rock surface was positive and electrons were injected from the electrode into the rock.

The rock rested on a 1.5-cm-thick Al metal plate, electrically insulated from the AVGR vacuum chamber by a block of solid wood but connected to the oscilloscope ground. The experiments were conducted in a residual gas pressure of 3-4 mbar achieved after 30 min of pumping. The vacuum, though modest, assured that the rocks were dry. The rock surfaces were smooth as cut with a diamond saw, but not polished.

For data acquisition two four-channel digital oscilloscopes were used in parallel: (1) a 200-MHz Tektronix oscilloscope, model 420A, for recording the EM emission from the three magnetic pick-up coils and the voltage of the top electrode and (2) a 500-MHz Tektronix oscilloscope, model 756, for recording the three capacitor signals and the voltage of the bottom electrode. The data acquisition was triggered through the AVGR electronics. Both oscilloscopes stored the data from the trigger point minus 5 ms until the buffer was full, typically ~30 ms after impact.

All shots were fired at normal incidence. Shots 1 and 3 served to test all channels and tune the settings so that the signals recorded by each sensor were strong enough and clearly resolved but not off-scale. Shot 2 was lost due to a triggering error. Shot 4 at 1.46 km/s produced usable data on all eight channels, while shot 5 at 1.79 km/s gave usable data on five of the eight channels. The shots, all fired at the same spot, led to the excavation of a near-cylindrical hole, ~10 mm wide, growing to a depth of ~50 mm and possibly deeper after shot 5. Shot 6 at 4.45 km/s gave usable data on all eight channels but caused three fissures to appear at roughly 120° on the surface of the block. Shot 7 at 5.64 km/s caused catastrophic fracture into three segments.

2.3. Samples

The low-velocity experiments were conducted with two rocks: (1) a whitish-gray speckled gabbro with phaneritic texture containing ~80% whitish plagioclase (bytownite with 88% An) and ~20% large, dark, elongate pyroxene (clinopyroxene « orthopyroxene) with thin augite exsolution lamellae, and (2) a dark, almost black diorite with phaneritic texture containing abundant orthopyroxene, often with very fine exsolution lamellae, clouded plagioclase (labradorite with 67% An), magnetite, minor hornblende and biotite and very minor K-feldspar and quartz. When impacted several times, the gabbro cores chipped more easily than the diorite cores.

The medium-velocity experiments were conducted with granite from Barre, Vermont. The granite is coarse-grained, light gray and shows no sign of texture that could lead to a preferred orientation of the quartz crystals. Having been stored in the laboratory for several months, the granite was air dry.

3. Results

3.1. Low-Velocity Impacts

When a steel ball hits the rock, several effects occur in rapid succession, variable from shot to shot, but displaying a recurring pattern. Figure 2a shows an experiment with a gabbro core, equipped with a photodiode at the front face (channel 4), a ring capacitor near the front (channel 2), and a plate capacitor at the back end (channel 3).

The moment of impact is marked by a short (10 μs), weak light blip (vertical arrow). About 150 μs after impact the ring capacitor, 10 mm from the impact point, begins to record a positive voltage that rises to above +400 mV. About 250 μs after impact the back end plate capacitor, 70 mm from the impact point, begins to show a positive voltage that rises to +40 mV. When the front ring capacitor voltages exceeds +400 to +450 mV (~450 μs after impact), light is emitted, much stronger and longer lasting than that at impact. This effect will be called the "delayed light." At the same moment the front capacitor voltage breaks down and may even go negative.

The same effects are even more clearly displayed in Figure 2b where a diorite core was used. Only the front capacitor

voltage (channel 3) and the light emission (channel 4) are shown. The impact light blip was not picked up, probably because the ricocheting steel ball blocked the light path. The dotted line on channel 3 traces the voltage at the front capacitor that may have reached values well above +400 mV without the intervening delayed light emission, causing it to break down abruptly. As in Figure 2a, when the delayed light emission occurs, the front capacitor voltage collapses and turns briefly negative. It recovers to around +300 mV and decays in an irregular manner that may contain some low frequency components.

In Figure 2c, also with the diorite core, the front ring capacitor was replaced by a magnetic pick-up coil, while leaving the photodiode at the front and the plate capacitor at the end in place. At impact, the coil registers an EM emission. Its intensity increases slightly at the delayed light emission. This is a recurring feature that is often observed and some times quite pronounced.

In Figure 3 the magnetic pick-up coil (channel 2) was moved along the axis and a contact ring electrode (channel 1) was installed at the front end, leaving the back end plate capacitor in place. Channel 3 records the back end capacitor voltage. Channel 4 records the light emission. What is different with respect to the configurations in Figures 2a-2c is that the rock core now is grounded at two places, first via the electrode across the 2.4-MΩ resistor and second at the grounding point about 2/3 down the length of the core. At impact, a 10-20 μs light blip occurs plus a sharp onset of EM emission that continues for several ms. The front end electrode records a positive voltage ~200 μs after impact, indicating that the elec-

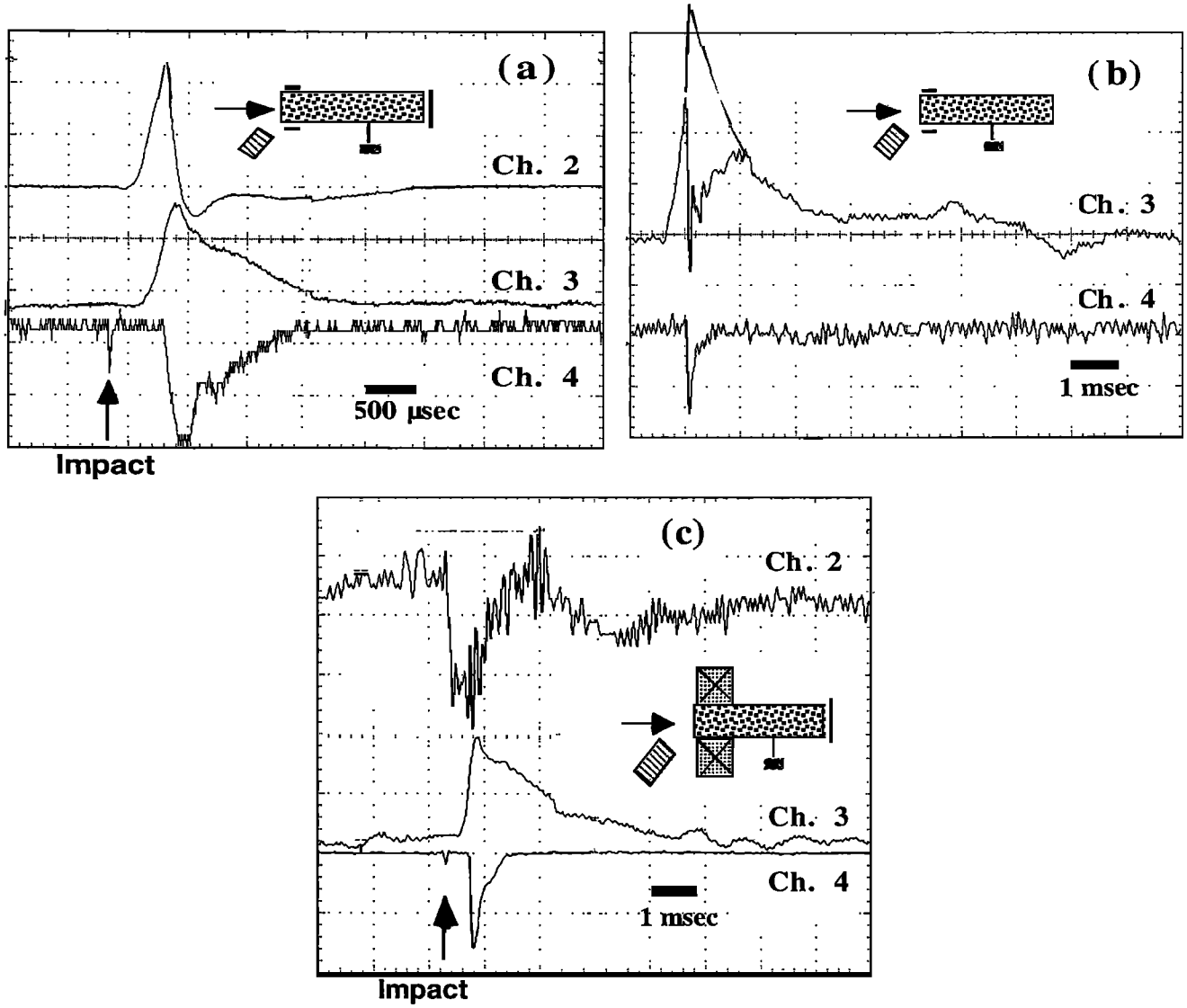

Figure 2. 100 m/s impact. (a) Gabbro core, 1/8-inch steel ball. Channel 2, front ring capacitor, 200 mV; channel 3, back end plate capacitor, 20 mV; channel 4, front end light emission, 200 mV. (b) Gabbro core, 3/16-inch steel ball. Channel 1, ring collector voltage, 400 mV; channel 2, magnetic field emission, 10 mV; channel 3, back end capacitor voltage, 20 mV; channel 4, front end light emission, 500 mV; (c) Gabbro core; 3/16-inch steel ball. Channel 1, ring collector voltage, 400 mV; channel 2, magnetic field emission, 10 mV; channel 3, back end capacitor voltage, 20 mV; channel 4, front end light emission, 500 mV.

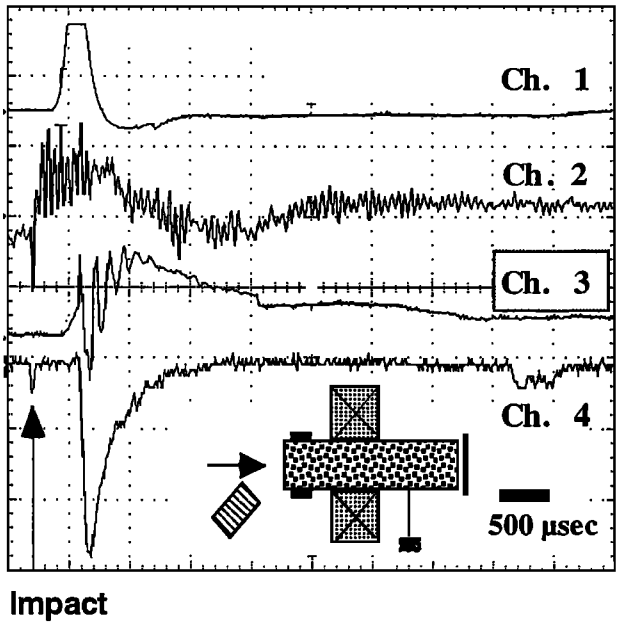

Figure 3. A 100 m/s impact. Diorite core; 3/16-inch steel ball. Channel 1, ring electrode voltage, 400 mV; channel 2, EM emission, 10 mV; channel 3, back end capacitor voltage, 20 mV; channel 4, front end light emission, 500 mV.

trode begins to inject electrons into the rock. The electron injection increases steeply with the voltage signal rising beyond +500 mV and eventually going off scale. The delayed light emission sets in sharply 400-420 µs after impact. At the same moment the positive voltage recorded by the back end capacitor (which had just started to rise) begins damped 8-kHz oscillations.

Voltage oscillations at the back end capacitor are seen in all experiments where the rock was grounded at more than one place. Examples are given in Figures 4a and 4b with a diorite core equipped with three ring electrodes in direct contact with the rock surface (channels 1-3), the back end capacitor, and the front photodiode. Because only four recording channels were available, we conducted two shots under otherwise identical conditions, switching channel 4 from the back end capacitor (Figure 4a) to the photodiode (Figure 4b).

In Figure 4a the moment of impact is moved off-scale to the left. The three electrode voltages rise simultaneously, indicating the time when all three electrodes begin to inject electrons into the rock. As the voltage at the first two electrodes reaches maximum and begins to break down (presumably because of the on-set of a delayed light emission), the voltage of the back end capacitor begins to oscillates wildly. The frequency, 40-45 kHz, is distinctly higher than in the case depicted in Figure 3. The oscillations decay over <1 ms. Concurrently, a faint 40-45 kHz ripple appears on the voltage signal recorded from the third electrode, closest to the grounding point, suggesting some kind of coupling between the

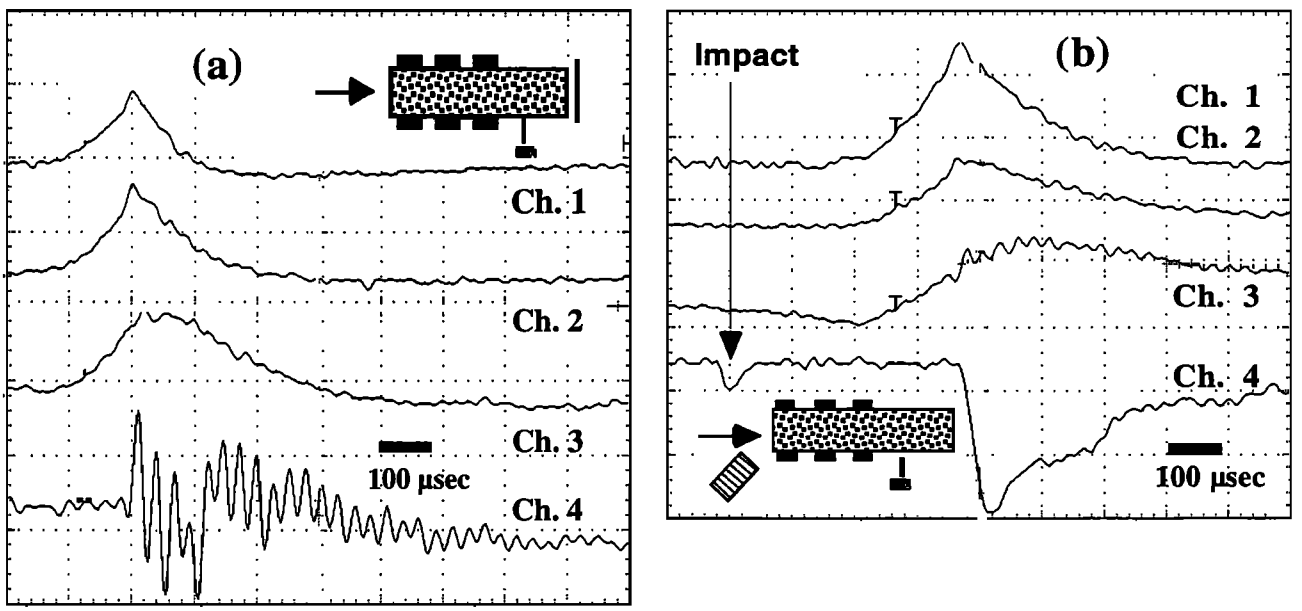

Figure 4. A 100 m/s impact. Diorite, 3/16-inch steel balls. (a) Channels 1-3, three ring collector electrodes, 500 mV, 100 mV and 20 mV, respectively; channel 4, back end capacitor voltage, 5 mV. Note the kilohertz oscillations of the back end capacitor voltage and the 38-kHz ripple on the three ring collectors after the onset of the light emission; (b) Channels 1-3, three ring collector electrodes, 500 mV, 100 mV and 20 mV, respectively; channel 4, front end light emission, 1 V. **Figure 5.** A 100 m/s impact. Diorite core, showing strong light emission from the front and occasional weak light emission from the back end. (a) Impacted by a 3/16-inch steel ball. Channel 1, front end light emission, 1 V; channel 2, magnetic field emission, 20 mV; channel 3, light emission from back end rim, 50 mV; channel 4, light emission from the back end center, 50 mV. (b) Impacted by a 1/4-inch steel ball. Channel 1, front end light emission, 4 V; channel 2, magnetic field emission, 40 mV; channel 3, light emission from back end rim, 5 mV; channel 4, light emission from back end center, 5 mV.

electron injection process and the electric field at the rock surface sensed by the back end capacitor.

The second shot is depicted in Figure 4b where channel 4 was used for the photodiode. A 20-30 μs impact light blip is clearly identified. It is followed 250 μs later by the simultaneous build-up of the voltage at the three contact electrodes, signaling electron injection into the rock. About 400 μs later a sudden, intense delayed light emission occurs. At the exact moment when the delayed light emission occurs, the voltage recorded by the first and second electrode voltage begins to break down. The third electrode, closest to the grounding point, registers the same faint 40-45 kHz ripple as in Figure 4a. The voltage oscillations indicate that when the rock core is in electrical contact with ground at more than one place and a positive charge appears at the rock surface some time after impact, electron injection at the different contact points occurs intermittently, in an oscillatory fashion. This effect will be more clearly demonstrated in the course of the medium-velocity experiments.

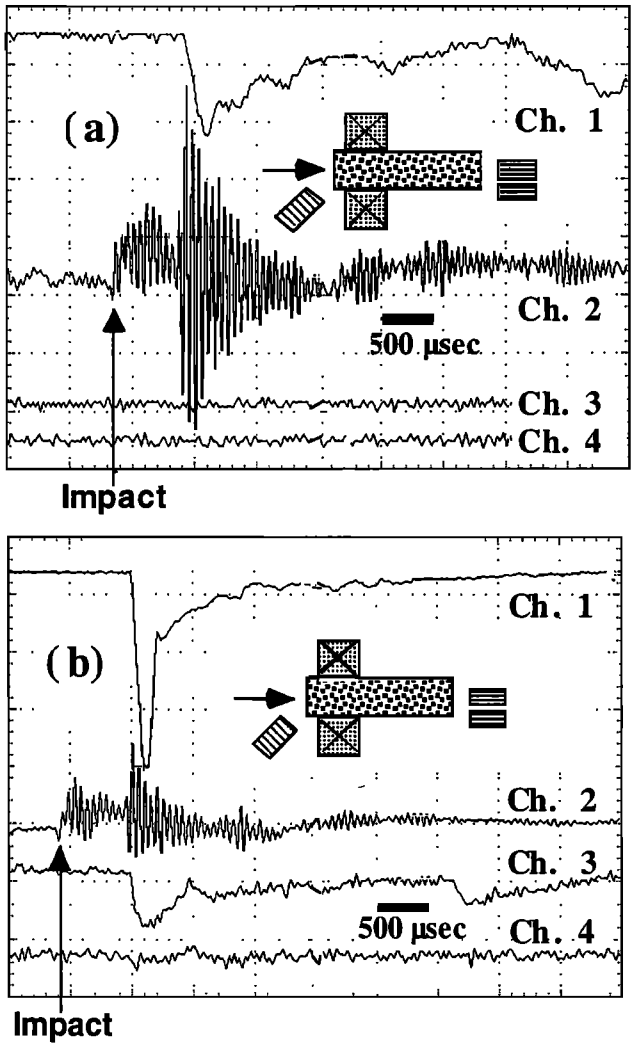

Figure 5. A 100 m/s impact. Diorite core, showing strong light emission from the front and occasional weak light emission from the back end. (a) Impacted by a 3/16-inch steel ball. Channel 1, front end light emission, 1 V; channel 2, magnetic field emission, 20 mV; channel 3, light emission from back end rim, 50 mV; channel 4, light emission from the back end center, 50 mV. (b) Impacted by a 1/4-inch steel ball. Channel 1, front end light emission, 4 V; channel 2, magnetic field emission, 40 mV; channel 3, light emission from back rim, 5 mV; channel 4, light emission from back end center, 5 mV.

To pursue this question further we configured a diorite core with a photodiode at the front to detect light from the front end (channel 1), a magnetic pick-up coil close to the front end (channel 2), and two photodiodes at the back to detect light from the back end directed at the rim of the core (channel 3) and at the flat center of the core (channel 4). The core was impacted repeatedly at 90 m/s, first with 3/16-inch, then with 1/4-inch steel balls, until it chipped and eventually fractured.

Figure 5a shows the results of a shot with a 3/16-inch steel ball. It produced a distinct onset of EM emission upon impact (vertical arrow) though the impact light blip was either too weak to be recorded or blocked by the ricocheting ball. About 500 μs after impact the delayed strong light emission occurred from the front end, accompanied by a strong burst in EM emission. The same EM emission response at impact and at the onset of the delayed light emission is seen in the shot depicted in Figure 5b, using a 1/4-inch steel ball. In both cases the front end light emission continued with variable intensity for over 3 ms, accompanied by variable EM emission. This correlation between delayed light emission and EM emission supports the contention that an electric discharge is the most likely cause. Repeatedly, a weak light signal was registered from the back end of the core, as illustrated in Figure 5b, always from the rim, never from the center. Within the time resolution of the experiment, the back end light emission occurs contemporaneous with the front end light emission. This suggests that the light emission is not directly controlled by the propagating charge (registered by the capacitive sensors) but by the potential that builds up over the entire rock surface as a result of the propagating charge.

The ensemble of the results obtained so far suggest that all low-velocity impacts, even those with the lightest steel balls, generated electrical charge carriers in the rocks. There seems to be no threshold for the appearance of charge carriers, though the limited range of the kinetic energy deposited into the rocks in this part of the impact experiments, 0.06-0.4 Joules, may have precluded the identification of such a threshold. Furthermore, the observations suggest that the charge carriers spread through the cores at a relatively high speed, in the range of 100-300 m/s. Their sign is positive. Since the carriers are obvious electronic in nature, a positive sign identifies them as defect electrons.

To demonstrate the effect of the charge cloud, an experiment was set up to test whether the rock becomes conductive as the charge carriers propagate. The configuration is depicted in the inset in Figure 6 (except for the magnetic pick-up coil). The sample consisted of a rectangular piece of diorite, 15 x 15 x 40 mm, with polished ends onto which 5-mm-diameter gold electrodes were sputtered; 25 V were applied across the long dimension, 40 mm, while the block was impacted from the side, normal to the applied electric field, using a 1/8-inch steel ball. The current flowing through the rock was determined by measuring the voltage drop across a 2.4-MΩ resistance R (Channel 3). In addition, the light emission was recorded from the rock face where the impact occurred (channel 1) and the EM emission, using a magnetic pick-up coil mounted at 90° with respect to both the externally applied electric field and the direction of the impact (channel 4).

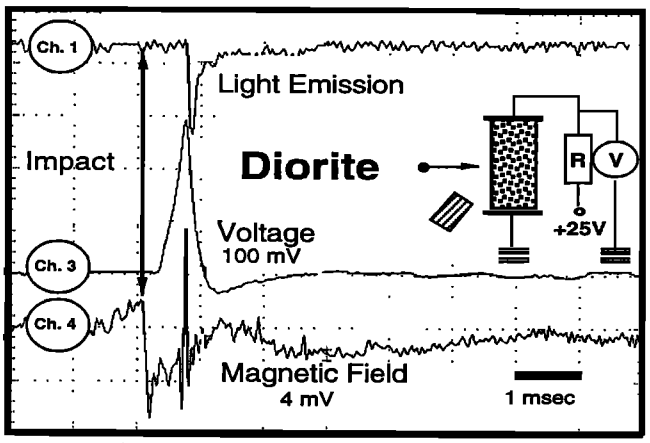

Figure 6. A 100 m/s impact. Cross current measurement with a rectangular piece of diorite impacted at right angle to the applied 25 V. Channel 1, light emission; channel 3, cross current; channel 4, EM emission (magnetic pick-up coil not shown in inset).

Figure 6 shows the sharp onset of EM emission that marks the impact. About 150 μs later, the voltage across the resistance R begins to rise, indicating a current that flows into the rock. Within 150 μs, about 300 μs after impact, a signal as high as 300 mV is recorded. The voltage increase abruptly ends when a sharp light pulse is emitted from the rock face, accompanied by a sharp EM pulse that lasts for <10 μs. The intensity of the emitted light decays rapidly, and so does the voltage across R. Within 200 μs the sign of the voltage reverses, indicating a reversal of the current flow, for example, that electrons leave the rock and reenter the electrodes. Both the voltage signal and the EM emission continue to reverberate for a few milliseconds. These observations confirm that as a result of the sudden stress load of the 90 m/s impact, charge carriers are generated, probably within a small volume near the impact point. The charge carriers then propagate through the rock. They cause the previously insulating rock to become briefly conductive, capable of supporting a cross current of electrons injected from the Au electrodes.

3.2. Medium-Velocity Impacts

The main questions addressed by the medium-velocity impacts are as follows: (1) Will the granite also generate positive holes when subjected to a sudden stress load? (2) Is the mode of activation of the charges different at high kinetic energies deposited into the rock? (3) How does the presence of piezoelectric quartz affect the measurements?

Figure 7 shows data recorded on the 200-MHz oscilloscope during shot 4 (1.46 km/s), the first shot for which complete data were obtained on all eight channels. The locations of the coils and the top contact electrode are indicated in the inset. The approximate time of impact is marked by the dotted vertical line. The data cover the first 5 ms after impact. Channels 1-3 registered the signals from the top, middle and bottom magnetic pick-up coils, the sensitivities of which were set at 200, 100, and 50 mV/div, respectively. Channel 4 registered the signal from the top contact electrode at 200 mV/division.

All three coils record EM emissions, though at different frequencies. The signal recorded by the plasma coil is relatively weak, suggesting that the 1.46 km/s impact did not produce the type of intense plasma plumes as high velocity or hypervelocity impacts do [*Crawford and Schultz*, 1988, 1991]. The EM emission of the impact plasma lasts for ~500 μs. The EM signal recorded by the middle coil lasts between 500 μs and 1 ms. The EM signal recorded by the bottom coil

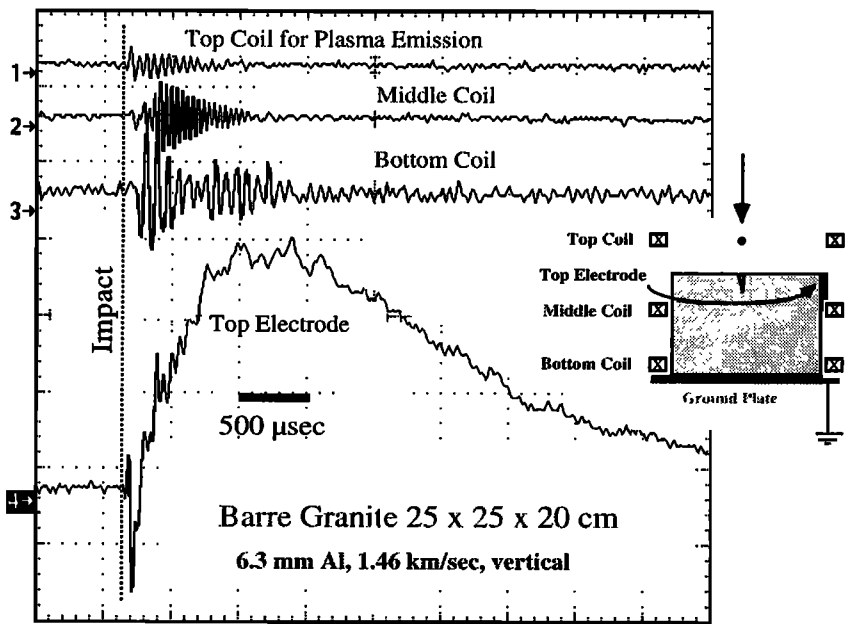

Figure 7. The 1.46 km/s impact of shot 4 on granite block with the signals from the three magnetic pick-up coils and the top contact electrode positioned as shown in the inset, using the 200-MHz oscilloscope model 420.

lasts for about 1.5 ms and continues to have a somewhat elevated noise level after the main signal has decayed.

The same EM signals as in Figure 7 are shown at higher time resolution in Figure 8a. Taking the first EM spike recorded by the plasma coil as the moment of impact, the coil at half height and the coil at the bottom begin registering EM emissions at slightly later times as marked by the arrows. The time-delayed onset of the EM signals indicates little or no "cross-talk" between the coils, meaning that the EM emissions registered by the middle and bottom coils are uncontaminated by the impact plasma. This is borne out by the clean ringing of the middle coil signal which reaches maximum intensity ~250 μs after impact and then decays exponentially within ~750 μs. The delayed arrival of the EM signals from the middle and bottom coils, about 35 μs and 65 μs after the plasma signal, suggests that these coils register an electric charge moving through the granite block. The front of this charge-generating process propagates at a much higher speed than observed during the low velocity impact experiments, at least 10 times as fast.

In all shots in the 1.5 km/s impact velocity range for which data are available the EM signals recorded by the middle and bottom coils were delayed by ~35 and 65 μs with respect to the EM signal from the plasma coil. When the impact velocity was higher, 4.45 km/s as in shot 6, the middle and bottom coil still receive their EM signals ~35 μs and 65 μs after the on-set of the plasma coil emission, respectively. The data for shot 6 at 4.45 km/s are shown in Figure 8b. The envelop of the plasma EM emission is quite regular, possibly because the previous shots had by then excavated a hole ~10 mm wide and 70 mm deep into the granite block which focussed the plasma plume into a narrow fountain. Shot 6 resulted in three vertical fissures, running through the granite block at ~120° with respect to each other. These fissures began to form after the 2 ms time window presented in Figure 8b. However, they did not yet lead to a disintegration of the block.

An example of EM emission when massive fracture occurs is shown in Figure 8c, presenting the data from shot 7 at 5.64 km/s. This shot caused the block to break into three sections along the fissures preformed during shot 6. The data from the

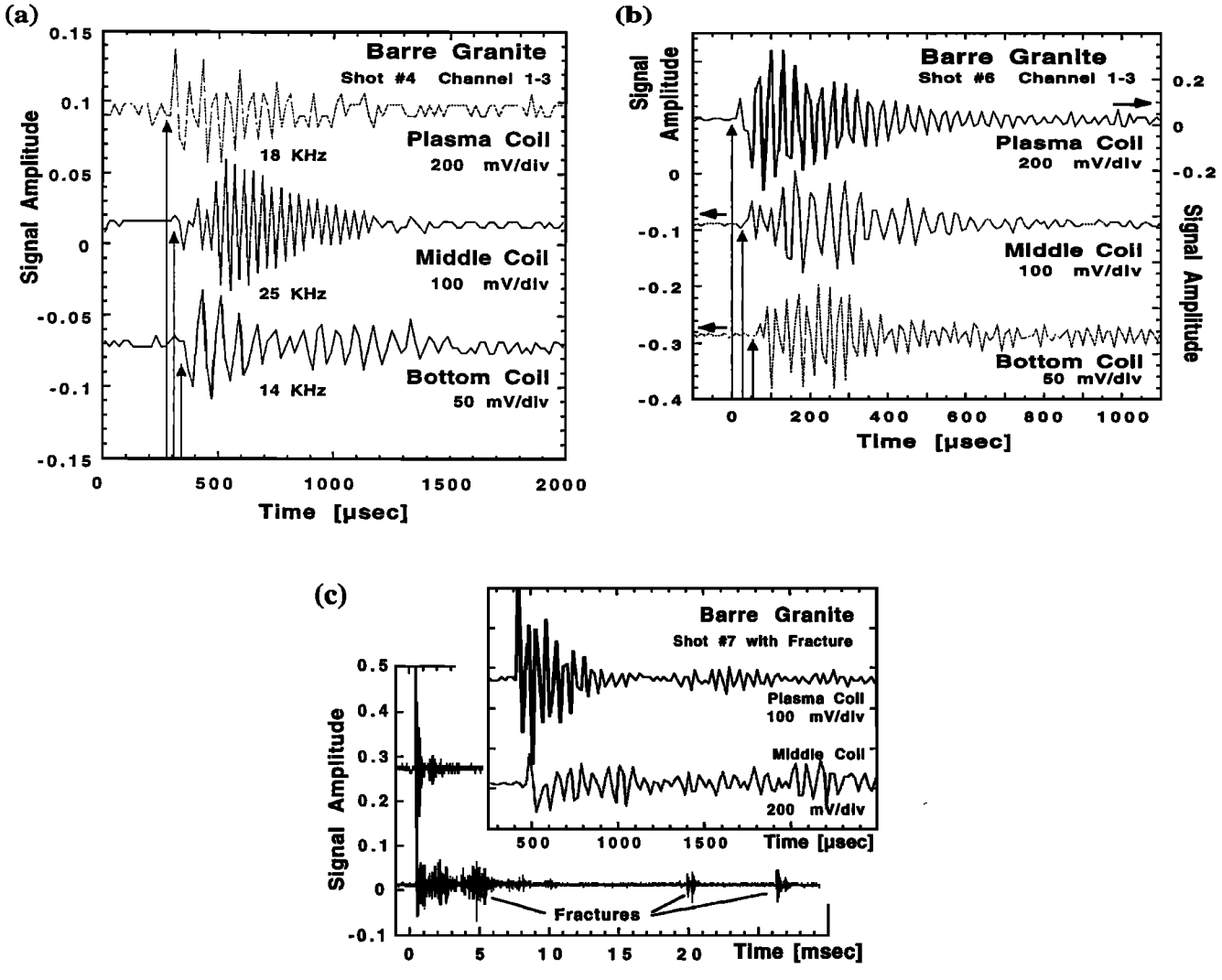

Figure 8. Electromagnetic emission as recorded by the magnetic pick-up coils after impact of the Al sphere (a) during shot 4 at 1.46 km/s, (b) during shot 6 at 4.45 km/s and (c) during shot 7 at 5.64 km/s which led to disintegration of the granite block.

bottom coil were lost. The EM emission recorded by the plasma coil and the middle coil is shown on two timescales, 30 ms in the main plot and 2.5 ms in the inset. The plasma coil registered an intense EM emission immediately after impact with some minor reverberation lasting ~2 ms, maybe because the plasma became entangled in the opening cracks of the disintegrating rock. The middle coil registered its first signal with the expected time delay of ~65 μs, followed by multiple bursts of EM emission, at 5, 20, and 26.5 ms, probably all associated with the opening and propagation of the cracks.

While the EM emission recorded by the magnetic pick-up coils indicates a rapidly moving charge or charge-generating process, the capacitive sensors register directly the charge on the granite surface and its sign. Figure 9a shows the voltage response of the three capacitive sensors arranged on one side of the granite block as depicted in the inset plus the voltage recorded by the bottom electrode, <1 cm from the grounded metal base. The time of impact is marked by the dotted vertical line. The response of the capacitive sensors is quite different from that encountered during the low velocity impact experiments. The signals arrive soon after impact, within 65 μs or less, though the distances from the point of impact to the sensors are ~15, 18, and 25 cm, respectively. This clearly indicates that the same process responsible for the EM emissions as shown in Figures 8a-8c is responsible for the charges recorded by the capacitor sensors. However, instead of a smoothly rising positive voltage as in the case of the low velocity experiments, the voltage signals begin with a series of short pulses. These early pulses last 20-30 μs. After ~500 μs when the EM emission has ceased and a large positive charge builds up in the rock, different oscillations take over. The amplitudes increase from the top to the bottom capacitive sensors. The bottom contact electrode displays particularly large amplitude variations, but none of the 20-30 μs pulses seen by the capacitive sensors within the first 500 μs.

In Figure 9b the data of shot 4 are replotted with higher time resolution. The inset in the lower right recapitulates the locations of the three capacitors and the contact electrode. The inset in the upper right plots the P and S wave velocity for Barre granite as a function of the confining pressure [*Christensen*, 1982]. Since the impact experiments were conducted in vacuum, the P and S wave velocities to be considered here are expected to lie in the ranges of 5.5-6 km/s and 3-3.4 km/s, respectively. As in Figure 7, the gray line marks the approximate time of impact as derived from the onset of the EM emission recorded by the plasma coil (Figure 8a).

Because the target is granite and contains quartz, we must be prepared to see piezoelectric effects during the propagation of the *P* and *S* waves. Indeed, the first signals recorded by the three capacitive sensors on the granite surface are short voltage pulses, 20-30 μs wide, beginning with a positive excursion, followed by a negative excursion. Because of the square cross section of the granite block, the distances from the point of impact to the three 20-cm-long, 1-cm-wide stripes used for the capacitive sensors are not constant. The distance to the top sensor varies from 12.5 to 17 cm (average ≈15 cm), that to the middle sensor from 15 to 23 cm (average ≈19), and that to the bottom sensor from 22 to 31 cm (average 27 cm). Within the accuracy of the measurements the arrival times of the first voltage pulse at the three sensor locations are delayed by ~20-30, 30-40 and 50-65 μs. These delays suggest that the signals are generated by a wave traveling downward through the rock at a speed close to that of the *P* wave, somewhat <6 km/s. This interpretation draws support from the fact that capacitor signals display a rapid inversion from positive to negative voltages such as one would expect from the compression and rarefaction phases of a passing *P* wave. The effect is particularly well seen in the voltage signals from the top and middle capacitive sensors in Figure 9b.

Thus, marking the first voltage signals received at the three capacitive sensors by solid circles, the solid line drawn through these signals in Figure 9b would correspond to the propagation of the *P* wave. Likewise, beginning with the second voltage signal received by the top capacitive sensor, a line can be drawn through a second train of voltage pulses, marked by solid circles and the dashed line, that corresponds to the S wave propagating downward at a speed close to or somewhat <3 km/s. Finally, the open circles and dotted lines in Figure 9b mark signals that may belong to the reflected *P* and *S* waves, though this assignment is tentative.

If the trains of the first voltage pulses recorded by the three capacitive sensors after impact are due to the piezoelectricity of quartz crystals at the rock surface that experience the passing *P* and *S* waves, these signals should last only as long as the transient stresses are applied. As the stresses go, the piezovoltage disappear instantly. Therefore all piezoelectric signals are expected to decay as rapidly as the *P* and *S* waves. Assuming that the sound waves reverberate in the 25 x 25 x 20 cm granite block over two to three reflections, each lasting <100 μs for the *P* wave and <200 μs for the *S* wave, the piezoelectric signals can be expected to decay within 500-700 μs. This time window agrees rather well with the duration of the EM emission recorded by the middle coil as shown in Figures 8a and 8b, suggesting that a large component of the EM emission comes from transient piezoelectric voltage pulses that are created by the reverberating *P* and *S* waves.

However, Figure 9a also shows that, while the piezosignals fade away within 700-800 μs after impact, the top capacitive sensor registers a positive potential that builds up over the same period of time, indicating a positive surface charge. The potential reaches nearly +400 mV within 700-800 μs and decays over the next 2 ms. The middle and the bottom capacitive sensors register similarly large positive signals, reaching +380 mV and +300 mV, respectively. They are overprinted by amplitude variations that increase in intensity from the top to the bottom sensor. The oscillations registered by all three capacitive sensors are inphase.

Thus the potentials recorded after medium-velocity impacts resemble those recorded after low-velocity impacts. In the latter case they were attributed to a charge cloud propagating from a small rock volume close to the point of impact. The difference to the 1.5 km/s impact experiment is that in the latter, the charge seems to build up simultaneously at all three sensor locations. Apparently, after the reverberations of the sound waves had died down, the granite block was left with activated positive holes throughout its volume. Given the 100-fold higher kinetic energy of the 1.5 km/s impact compared to the earlier 100 m/s impacts, it is likely that the positive holes were generated in the wake of the sound waves.

The amplitudes of the overprinted oscillations increase the closer the sensor is to the grounded metal base plate. The amplitude variations recorded by the three capacitive sensors are in phase, suggesting that they reflect electric field variations that occur simultaneously at all three sensor locations. Likewise, the weak "ripple" in the top contact electrode signal is in phase with the large amplitudes of the bottom contact electrode signal. The question arises: What is the cross relationship between these two sets of signals?

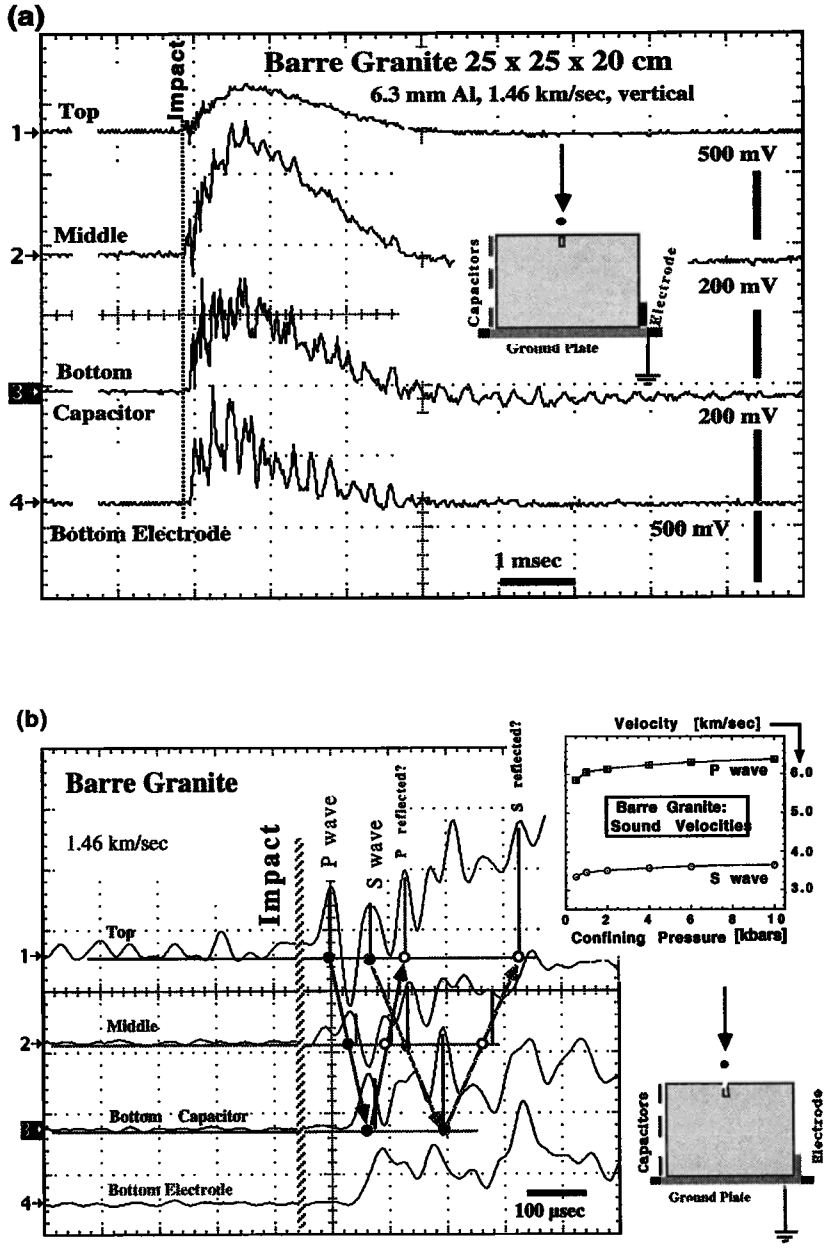

Figure 9. The 1.46 km/sec impact of shot 4 on the granite block. (a) Signals from the three capacitive sensors and the bottom contact electrode positioned as shown in the inset, using the 500-MHz oscilloscope model 754. (b) Initial arrival of the signals at higher time resolution with tentative assignment of the short voltage pulses to piezoelectric signals arising from the passing of the incoming and reflected(?) **P** and **S** waves. Inset shows velocities of the **P** and **S** waves in Barre Granite as a function of the confining pressure after *Christensen* [1982].

In Figure 10 we plot jointly the bottom capacitive sensor voltage and the bottom contact electrode voltage, the latter indicating the current injected into the rock. Both sensors are located ~1 cm from the grounded metal base plate but on opposite faces of the granite block. The double arrows indicate signals that are generally out of phase. This is consistent with the concept developed above for the low-velocity impacts: When the potential at the rock surface exceeds the barrier height, the contact electrode will inject electrons into the rock. Following electron injection, the positive potential at the rock surface breaks down. As soon as the surface potential drops below the barrier height, electron injection shuts off, giving the rock surface time to recover its potential as long as positive holes still arrive from inside the bulk. The result is that the system goes into oscillations with the signals of the capacitive sensors and contact electrodes being out of phase.

4. Discussion

The low- and medium-velocity impact experiments described here have proven to be a valuable tool to study elec-

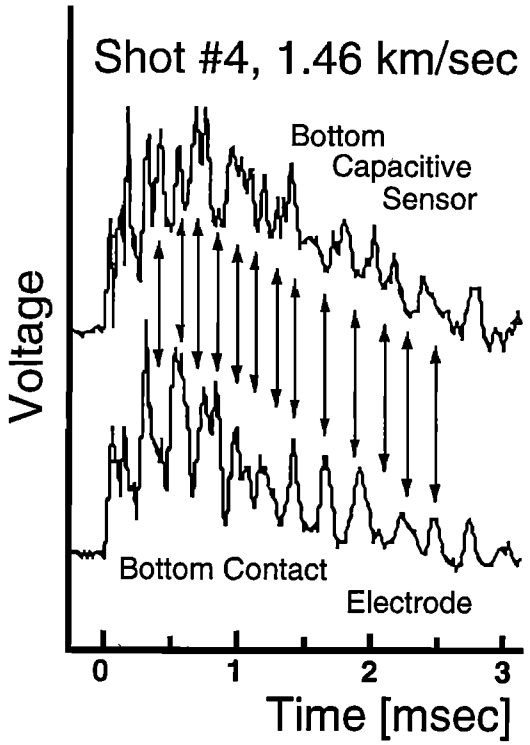

Figure 10. Out-of-phase correlation between the voltage signal as recorded by the bottom capacitive sensor (top trace) and the electron injection into the rock as recorded by the bottom contact electrode (bottom trace).

trical processes in rocks. By timing the impacts and measuring the subsequent events with microsecond ot millisecond resolution, processes activated by a sudden stress load can be identified. The insight thus gained may shed light on electrical, electromagnetic, and luminous phenomena reportedly associated with earthquake activity.

4.1. Recapitulation

To recapitulate, when common igneous rocks are subjected to the sudden stress load of an impact event, they generate highly mobile charge carriers. The charge carriers are electronic in nature. They spontaneously appear upon impact, propagate, and disappear after a few milliseconds. They cause transient electrical potentials at the rock surface. They can be reactivated by repetitive impacts. They emit electromagnetic (EM) signals and visible light. In the "as received" rocks they exist in a dormant form that is electrically inactive. At low impact energy the charges appear in a small volume close to the impact point. The low kinetic energy of these impacts suggests that the dormant precursors are easy to activate. At higher kinetic energies the charge carriers seem to fill the entire rock volume, presumably because they are activated in the wake of the more energetic sound waves.

Since the charge carriers are electronic, it is of diagnostic value to know that they are positive. They are holes as argued in section 3, specifically positive holes in the O 2p-dominated valence band of the constituent minerals, equivalent to O^- in the O^{2-} matrix. Their electrically inactive, dormant precursors should then consist of positive hole pairs, PHPs, chemically equivalent to peroxy links in the structures of the minerals, O^-–O^- or $O_3X/^{OO}\backslash XO_3$ with $X = Si^{4+}$, Al^{3+}, etc. The PHPs are believed to have been introduced into nominally anhydrous minerals through dissolution of small amounts of H_2O and subsequent redox conversion of O_3X-OH pairs into $O_3X/^{OO}\backslash XO_3$ plus H_2 as described by equations (1)-(4).

Normally, igneous rocks such as gabbro, diorite and granite are good insulators, especially when dry and at ambient temperature. Numerous studies have been published on the electrical conductivity of such rocks under a wide variety of conditions: temperature, atmosphere, confining pressure etc. [e.g. *Shankland*, 1981; *Shankland and Ander*, 1983]. None of these studies, though carefully conducted and controlled, seem to have produced evidence for the highly mobile, powerful electrical charge carriers that show up so prominently in the impact experiments described here.

This is reminescent of a situation encountered during a study of the model insulator MgO and its electrical conductivity as a function of temperature [*Kathrein and Freund*, 1983]. MgO had long been considered an excellent insulator up to temperatures above 700°C, the onset of ionic conductivity [*Sempolinski and Kingery*, 1980; *Wuensch et al.*, 1973]. There were hints of an unusual orders of magnitude increase in the conductivity in the 400-700°C interval but nobody pursued these leads because it could be shown that this enhanced conductivity was confined to the surface and therefore looked like being caused by some kind of "dirt." Upon heating the MgO crystals long enough to temperatures well above 700°C, the enhanced surface conductivity disappeared and the question seemed settled for good. A similar orders-of-magnitude enhancement of the electrical conductivity below 700°C was observed during the study of single crystals of upper mantle olivine by *Constable and Duba* [1990]. As in the case of MgO, the conductivity seemed confined to the crystal surface. Upon prolonged heating in a 1:1 CO/CO_2 gas mixture deemed representative the upper mantle environment, the enhanced surface conductivity disappeared, leading *Constable and Duba* [1990] to suggest that it was caused by a thin film of carbon vapor deposited from the CO/CO_2 gas mixture.

Meanwhile evidence, both theoretical [*King and Freund*, 1984] and experimental [*Freund et al.*, 1993], had been accumulating that MgO and probably also upper mantle-derived olivine crystals contain peroxy anions and peroxy links respectively, and that these represent positive hole pairs, PHPs, capable of dissociating and releasing highly mobile positive hole charge carriers. The predicted behavior of these charge carriers was unlike that of any other charge carriers studied until then. Their most characteristic and also most easily misinterpreted property derives from their mutual repulsion in the bulk that "pushes" them to the surface. The resulting surface layer is expected to exhibit enhanced conductivity. At the same time, because a positive hole represents an O^- in an O^{2-} matrix, and an O^- is an oxidizing radical, its chemical reactivity needs to be taken into consideration. Allowing an olivine crystal with thermally activated O^- charge carriers at its surface to react with a CO/CO_2 gas mixture at 700°C will lead to the annihilation of the positive holes, $CO + 2\ O^- = CO_2 + O^{2-}$. Using a similar reaction, $CH_4 + O^- = \bullet CH_3 + OH^-$ where $\bullet CH_3$ represents the gas-phase methyl radical, the O^- in olivine can in fact be titrated, using dielectric polarization to monitor the reaction [F. Freund, unpublished results, 1995].

As mentioned in section 3 the idea for the impact experiments came from the observation that positive hole-type charge carriers could be mobilized in MgO and olivine crys-

tals by the acoustic waves generated during brittle fracture [*Dickinson et al.*, 1986]. It was therefore reasonable to attempt to activate the same charge carriers through the acoustic waves of an impact event. The richness of the phenomena observed, electric, electromagnetic and luminous, validate the approach, though many details are still far from clear.

4.2. Positive Holes and Electron Injection

On the basis of the available impact data, a consistent picture emerges as far as the three types of rocks are concerned, quartz-free gabbro, low-quartz diorite and quartz-rich granite, that were included in this first series of impact experiments. They all display a behavior that is consistent with the appearance of positive hole charge carriers immediately after impact. In the case of the low velocity impact experiments, depositing 0.06-0.4 J of kinetic energy into the rock cores, the activation seems to be confined to a small volume near the impact point. The small light blip marking the impact is probably a triboluminescence phenomenon, arising from electron-hole pairs created during the rapid movement of dislocations and their radiative recombination [*Bräunlich et al.*, 1979]. From this source volume the positive holes propagate as a charge front. They cause EM emission, positive potentials, and light emission. In the case of the medium-velocity impact experiments, depositing ~40 J into the granite block, the activation of the positive hole charge carriers most likely occurs in the wake of the *P* or *S* waves. After the initial EM signals and the transient voltages (believed to be piezoelectric signals due to the propagating *P* and *S* waves) have died down, the capacitive sensors register the buildup of a pervasive positive charge, while the contact electrodes indicate pulses of electrons flowing into the rock for ~3 ms.

The correlation between surface potential and current into the rock provides support for positive holes as charge carriers activated by the impacts. Injection of electrons from metal contacts into the rock can only occur when the potential on the rock surface exceeds the barrier height at the metal-to-semiconductor interface. The barrier height is not exactly known

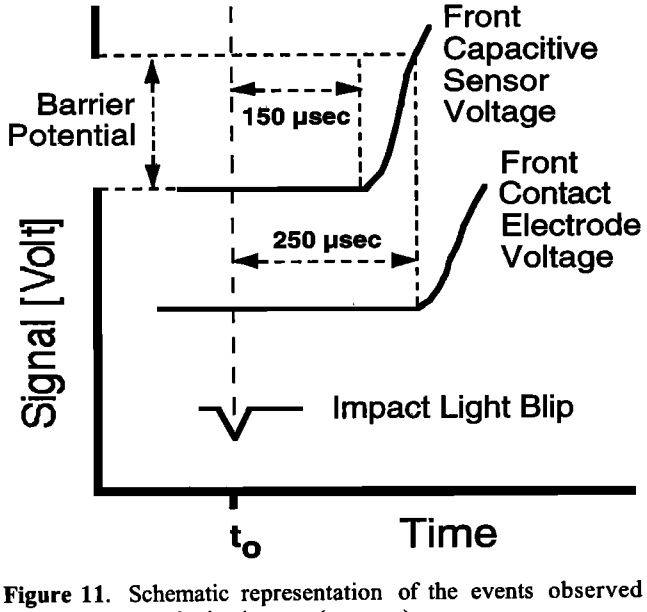

Figure 11. Schematic representation of the events observed following low-velocity impact (see text).

but typically of the order of a few hundred mV [*Kittel*, 1980]. To illustrate this process with reference to the low velocity impact experiments, Figure 11 indicates schematically the impact light blip at t_0 (bottom) and the arrival of the charge cloud at the capacitive sensor about 150 µs later (top). The potential at the rock surface builds up and reaches after some time, say 100 µs, the threshold high voltage that allows electrons at the metal-to-insulator contact to overcome the barrier potential. At this moment, electrons begin to flow from the contact electrode into the rock (middle). Thus the signal recorded by a contact electrode (Figures 2a, 2b, and Figure 3) will always rise later than the signal recorded by a capacitive sensor at the same location (Figures 4b and 5).

Figure 12 sketches the sequence of events that take place during a medium-velocity impact with emphasis on the surface potential recorded by the capacitive sensors and the current measured by the contact electrodes. In Figure 12a the impact occurs, sending acoustic waves into the rock. In Figure 12b positive holes, symbolized by dots, become momentarily activated in the entire rock volume. In Figure 12c, due to mutual repulsion, the positive holes diffuse outward toward the surface as indicated by the arrows. In Figure 12d the positive potential that builds up at the rock surface leads to the injection of electrons, *e'*, from both the grounded metal base plate and the contact electrodes.

Figure 13 follows the evolution of the signals in greater detail. Figure 13 (top) shows the granite block with the bottom capacitive sensor recording the voltage V and the bottom electrode recording the current I near the grounded bas plate. On the left the initial state is depicted, assuming that after passage of the acoustic waves, the rock volume is uniformly filled with mobile positive hole charge carriers. The initial state evolves toward the final state depicted on the right where the positive holes have come to the surface forming a positively charged surface layer balanced by a negatively charged interior. If the speed of propagation of the positive holes is of the order of 100 m/s, a block of granite measuring 25 x 25 x 20 cm can be expected to reach the final state within ~1-2 ms.

The three panels in Figure 13 (middle) depict from top to bottom: (1) the surface potential as it would be expected to build up during the transition from initial to final state if the granite block were electrically isolated; the dashed line at V_i marks the threshold voltage above which electron injection can occur across the metal-to-insulator contact; (2) the surface potential as recorded by the capacitive sensor, and (3) the injection current as recorded by the contact electrode. Each time the surface potential reaches the threshold value of V_i, electron injection occurs and the potential breaks down. This in turn shuts off the electron injection and allows the surface potential to recover. As the final state is approached, the time needed to reach V_i becomes longer, causing the oscillations to slow down. Eventually, the surface potential can no longer reach the V_i value and the electron injection stops abruptly. The process repeats itself giving rise to the out-of-phase oscillations of the capacitor and electrode signals as shown in Figure 10. In Figure 13 (bottom) the frequency of oscillation (in kHz) for the surface potential (diamonds) and the injection current (solid dots) is plotted versus time. The shaded area covers the first 700 µs during which the acoustic waves still reverberate in the block. This period is followed by 1-2 ms during which the frequency decreases from values between 5-10 kHz and 3-4 kHz.

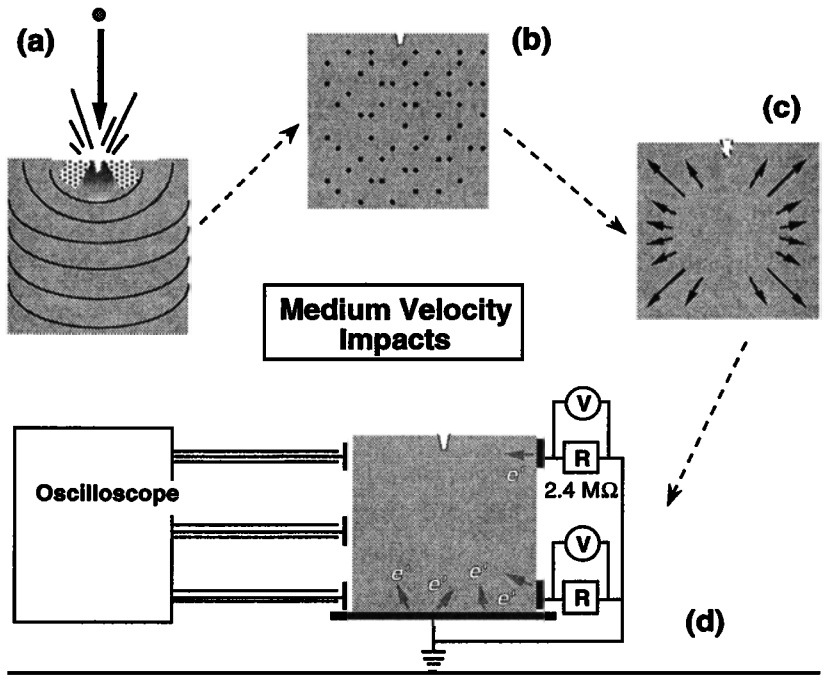

Figure 12. Cartoon of the processes taking place in rapid succession in the granite block following a medium velocity impact. (a) Impact and propagation of the sound waves. (b) Rock volume filled with positive hole charge carriers activated in the wake of the sound waves. (c) Diffusion of positive holes to the surface due to mutual repulsion in the bulk. (d) Injection of electrons from the base plate and contact electrodes leading to oscillations.

4.3. Application to Electrical Phenomena Related to Earthquakes

The experiments reported here provide evidence that common igneous rocks contain dormant electronic charge carriers that can be activated by sound waves. These charge carriers are positive holes, and they are unusual in many respects. Representing defect electrons in the O 2p-dominated valence band of the constituent silicate minerals, chemically O^- in an O^{2-} matrix, they are able to propagate through rocks over macroscopic distances with little apparent scatter or attenuation at the grain boundaries. In their electrical inactive, dormant state these charge carriers probably consist of positive hole pairs, PHPs, chemically equivalent to peroxy links, $O_3X/^{OO}\backslash XO_3$, for example, two O^- joint in a rather unstable O^-–O^- bond. This electronic defect may be universally present in nominally anhydrous minerals that crystallize in H_2O-laden magmas or H_2O-laden metamorphic environments and hence in most common igneous and high-grade metamorphic rocks.

The observation most relevant to earthquake-related issues is that sound waves can activate peroxy links and generate mobile positive hole charge carriers. It is currently unknown whether a clear threshold exists for the minimum kinetic energy to be deposited into the rocks in order to activate the mobile positive holes. Even the low velocity impacts with small steel balls produced detectable electrical, EM, and luminous effects as shown in Figure 2a and Figure 3, depositing into the rock 0.06 J or less considering that some of the kinetic energy was certainly carried away by the ricocheting steel balls. Maybe the activation of the peroxy links and mobilization of the positive holes occurs under any conditions that cause dislocations to move rapidly. In this case the threshold energy for the positive hole activation would be very low and could be achieved in a rock volume that undergoes microcracking during the dilatancy stage prior to an earthquake. As microcracks open and close in rapid succession throughout the stressed rock volume, each would cause rapid dislocation movements and generate tiny clouds of positive holes. As an ensemble, these clouds could generate enough charge carriers throughout the rock volume so that the resistivity of the rock changes with time in the manner depicted in Figure 1.

Molchanov and Hayakawa [1998b] introduce the concept of "electrification" by microfracturing as a possible mechanism for low-frequency EM emissions before and after earthquakes. If microcracks rapidly open and close in different parts of the rock, each generating microcurrents, they are assumed to "electrify" the regions and thereby produce a wideband EM noise. Without mobile charges, however, the model may be flawed because currents associated with microfracture are self-canceling and do not result in net charges. If, on the other hand, the charge carriers are positive holes, generated in the stressed rock and capable of propagating at speeds comparable to those determined from the impact experiments described here, rapid fluctuations in the charge carrier density are expected to occur between different parts of the rock volume. The fluctuations and the currents that they produce are expected to generate a wideband EM noise or discrete pulsations as observed during the December 7, 1988, M_s=7 Spitak, Armenia, earthquake [*Kopytenko et al.*, 1993].

With the knowledge that positive holes may be generated in rocks we can go one step further and address the phenomenon of earthquake lights. Reported in folklore [*Tributsch*,

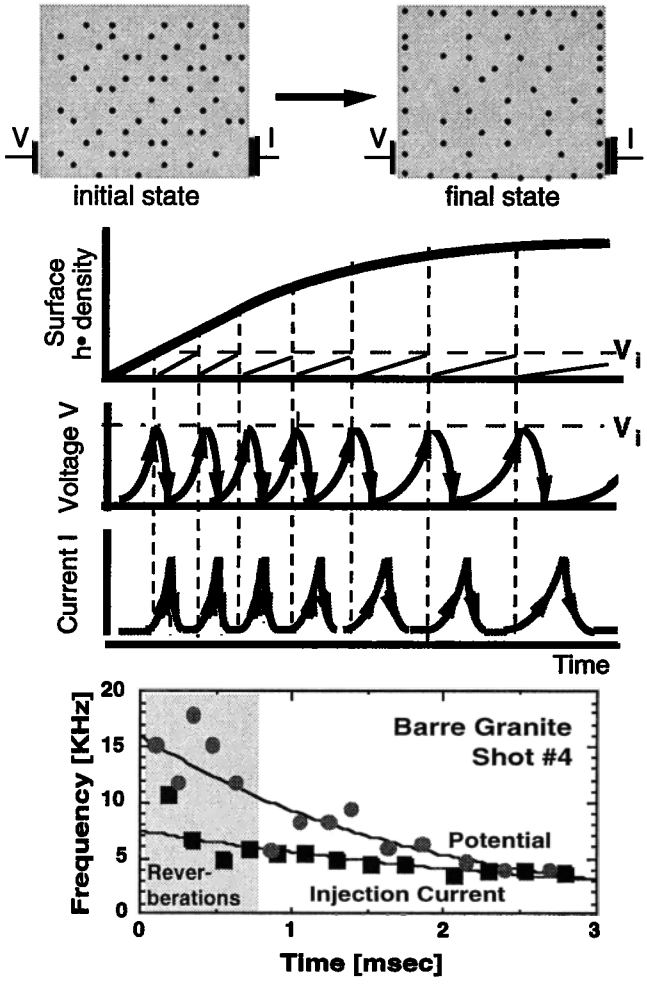

Figure 13. (top) Cartoon of the transition from (left) the initial state in which the rock volume is uniformly filled with positive hole charge carriers to (right) the final state in which the positive hole charge carriers have redistributed to form a positive surface charge, balanced by a negative interior. The capacitor sensor recording the surface potential V and the contact electrode recording the current I injected in to the rock are indicated. (middle) From top to bottom, surface charge density as it may develop as a function of time, if the system were unperturbed. (V_i marks the threshold potential at which current injection occurs.) Surface potential V building up repeatedly to the limit of V_I and then breaking down. Pulses of injection current I beginning each time at V_I and breaking down as the surface potential breaks down. (bottom) Frequency of the surface potential and of the injection current pulses using the data from Figure 11. The time period < 700 μs (shaded) is probably "contaminated" by reverberation of the acoustic waves before they dissipate in the block.

1983], many times in the scientific literature [*Derr*, 1973], and photographed during the 1966 Matushiro earthquake, Japan [*Derr*, 1986], earthquake lights have remained a contentious issue. The reason is that no mechanism was known that could reasonably explain electric discharges at the rock-to-air interface and the appearance of "St. Elmo's fire." Neither piezoelectricity from quartz-bearing rocks [*Finkelstein et al.*, 1973; *Nitsan*, 1977] nor sonoluminescence [*Johnston*, 1991] nor a fluid-driven dilatancy model [*Nur*, 1974] provides a physical concept that satisfies the conditions under which these luminous phenomena seem to occur.

When a positive hole cloud generated deep in the crust expands and reaches the surface, for example, the surface-to-air interface with its discontinuous dielectric contrast, theory predicts [*King and Freund*, 1984] and the observations reported here confirm (1) the formation of a thin surface charge layer, (2) the formation of a surface potential in the range of a few hundred mV, and (3) the appearance of very high electric fields at the surface. At relatively modest charge carrier densities of 100 ppm (10^{18} cm^{-3}), a surface potential of the order of 400 mV seems enough to initiate electric discharges, attendant light emission, and bursts of EM radiation. The discharges probably occur at the rim and the edges where the electric field is highest. The photographs of earthquake lights during the 1966 earthquake swarm at Matsushiro, Japan, show the hilltops illuminated [*Derr*, 1986]. consistent with an electric charge that causes the highest electric fields at the peaks of the mountains. In view of what we have learned through the impact experiments described here, it appears plausible that the charge carriers responsible for the earthquake lights during the 1966 Matsushiro event and on other occasions might have been positive holes, activated by the seismic waves.

Though we still lack experimental data on the role of water as a pore-filling liquid or as intergranular films, having recognized the existence of positive hole charge carriers opens a door to a new interpretation. Regardless whether water attenuates the charges as they propagate through a rock, leaves them unaffected or even enhances their passage, positive holes deserve further attention.

Acknowledgments. This work was performed without formal funding support. My thanks go to Jerome G. Borucki (NASA Ames Research Center) for his early involvement in sample preparation and data acquisition, to Michael Brunetti (California Monument, Inc.) and Michael J. Causi (Cañada Marble and Granite) for cutting rocks, to Bruce W. Fouke (University of Illinois at Urbana-Champaign) for petrographic analyses, and J. Thomas Dickinson (Washington State University) for constructive criticism at a crucial time of the experiments. Peter H. Schultz (Brown University) generously provided access to the NASA AVGR. Kraig Moll (Tektronix Instruments) made the four-channel 500 MHz oscilloscope available for the week of medium-velocity impact experiments. Scott Hubbard and Douglas O'Handley (both NASA Ames Research Center) provided help through the NASA Ames Astrobiology Academy. Alexander S. Bradley (Harvard University and student participant in the Astrobiology Academy 1998 Summer program) contributed to the data analysis. As reviewers, Malcolm Heggie (University of Exeter, U.K.) and Didier Sornette (University of California, Los Angeles) provided constructive criticism that helped improve the manuscript.

References

Bell, D.R., and G.R. Rossman, Water in Earth's mantle: The role of nominally anhydrous minerals., *Science, 255*, 1391-1397, 1992.

Bernabé, Y., Streaming potential in heterogenous networks, *J. Geophys. Res., 103*, 20,827-20,841, 1998.

Bernard, P., Plausiblity of long distance electrotelluric precursors of earthquakes, *J. Geophys. Res., 97*, 17,531-17,546, 1992.

Bilichenko, S.V., F.S. Iljin, and E.F. Kim, ULF response of the ionosphere for earthquake preparation processes, *Dokl. Acad. Nauk USSR, 311*, 1077-1080, 1990.

Bishop, J.R., Piezoelectric effects in quartz-rich rocks, *Tectonophysics, 77*, 297-321, 1981.

Bolt, B.A., *Earthquakes*, W. H. Freeman, New York, 1988.

Borevsky, L., S. Milanovsky, and L. Yakovlev, Fluid-thermal regime in the crust-superdeep drilling data, in *World Geothermal Congress*, edited by E. Barbier, G. Frye, E. Iglesias, and G. Palmason, pp. 975-981, Int. Geotherm. Assoc., Auckland, New Zealand, 1995.

Brady, B.T., and G.A. Rowell, Laboratory investigation of the electrodynamics of rock fracture, *Nature, 321*, 488-492, 1986.

Bräunlich, P., P. Kelly, and J.-P. Fillard, Thermally stimulated luminescence and conductivity, in *Thermally Stimulated Relaxation in Solids*, edited by P. Bräunlich, pp. 35-91, Springer-Verlag, New York, 1979.

•Chmyrev, V.M., V.N. Isaev, S.V. Bilichenko, E.P. Trushkina, and G. Stanev, Electric fields and hydromagnetic waves in the ionosphere above an earthquake center, *Geomagnet. Aeronom., 26*, 1020-1022, 1986.

Christensen, N.I., Seismic velocities, in *Handbook of Physical Properties of Rocks*, vol. II, pp. 1-228, CRC Press, Boca Raton, Fla., 1982.

Constable, S., and A. Duba, Electrical conductivity of olivine, a dunite and the mantle, *J. Geophys. Res., 95*, 6967-6978, 1990.

Crawford, D.A., and P.H. Schultz, Laboratory investigations of impact-generated magnetic fields, *Nature, 336*, 50-52, 1988.

Crawford, D.A., and P.H. Schultz, Laboratory investigations of impact-generated plasma, *J. Geophys. Res., 96*, 18,807-18,817, 1991.

Cremer, D., General and theoretical aspects of the peroxide group, in *The Chemistry of Functional Groups, Peroxides*, edited by E. S. Patai, pp. 1-79, John Wiley, New York, 1983.

Cress, G.O., B.T. Brady, and G.A. Rowell, Sources of electromagnetic radiation from fracture of rock samples in the laboratory, *Geophys. Res. Lett., 14*, 331-334, 1987.

Davis, K., and D.M. Baker, Ionospheric effects observed around the time of the Alaskan earthquake of March 28,1964, *J. Geophys. Res., 70*, 2251-2253, 1965.

Deb, B.M., and A.N. Chandorkar, Theory of hopping transport of holes in amorphous SiO_2, *J. Appl. Phys., 77*, 5248-5255, 1995.

Derr, J.S., Earthquake lights: A review of observations and present theories, *Bull. Seismol. Soc. Am., 63*, 2177-21287, 1973.

Derr, J.S., Luminous phenomean and their relationship to rock fracture, *Nature, 321*, 470-471, 1986.

Dickinson, J.T., L.C. Jensen, M.R. McKay, and F. Freund, The emission of atoms and molecules accompanying fracture of single-crystal magnesium oxide, *J. Vac. Sci. Technol. A, 4*, 1648-1652, 1986.

Dickinson, J.T., L.C. Jensen, and M.R. McKay, Neutral molecule emission from the fracture of crystalline magnesium oxide, *J. Vac. Sci. Technol. A, 5*, 1162-1168, 1987.

Dieckmann, R., C.A. Witt, and T.O. Mason, Defects and cation diffusion in magnetite (V): Electrical conduction, cation distribution and point defects in $Fe_{3-}\ O_4$, *Ber. Bunsen Ges. Phys. Chem., 87*, 495-503, 1983.

Dobrovolsky, I.P., N.I. Gershenson, and M.B. Gokhberg, Theory of electrokinetic effects occurring at the final stage in the preparation of a tectonic earthquake, *Phys. Earth Planet Inter., 57*, 144-156, 1989.

Draganov, A.B., U.S. Inan, and Y.N. Taranenko, ULF magnetic signatures at the Earth surface due to ground water flow: A possible precursor to earthquakes, *Geophys. Res. Lett., 18*, 1127-1130, 1991.

Drobzhev, V.I., V.M. Krasnov, and R.M. Salihov, About ionospheric perturbation associated with earthquake and explosions, *Izv. Vyssh. Uchebn. Zaved.Radiofizika, 21*, 1862-1863, 1978.

Edwards, A.H., and W.B. Fowler, Theory of the peroxy-radical defect in a-SiO_2, *Phys. Rev. B, 26*, 6649-6660, 1982.

Eiby, G.A., *Earthquakes*, Van Nostrand Reinhold, New York, 1980.

ELEKTB Groups: KTB and the electrical conductivity of the crust, *J. Geophys. Res., 102*, 18,289-18,305, 1997.

Emmermann, R., and J. Lauterjung, The German Continental Deep Drilling Program KTB: Overview and major results, *J. Geophys. Res., 102*, 18,179-18,201, 1997.

Enomoto, Y., and H. Hashimoto, Emission of charged particles from indentation fracture of rocks, *Nature, 346*, 641-643, 1990.

Finkelstein, D., U.S. Hill, and J.R. Powell, The piezoelectric theory of earthquake lightning, *J. Geophys. Res., 78*, 992-993, 1973.

Fraser-Smith, A.C., ULF, ELF, and VLF electromagnetic field observations during earthquakes: Search for precursors, in *Low Frequency Electrical Precursors: Fact of Fiction?*, edited by S.K. Park et al., pp. 70-73, Nat. Sci. Found., National Earthquake Hazard Reduction Program, Washington, D.C., 1992.

Fraser-Smith, A.C., A. Bernardi, P.R. McGill, M.E. Ladd, R.A. Helliwell, and O.G. Villard, Low-frequency magnetic field measurements near the epicenter of the M_s=7.1 Loma Prieta earthquake, *Geophys. Res. Lett., 17*, 1465-1468, 1990.

Freund, F., and J.G. Borucki, Charge carrier generation and charge cloud propagation following 100 m/sec impacts on igneous rocks, in *Atmospheric and Ionospheric Electromagnetic Phenomena Associated With Earthquakes*, edited by M. Hayakawa, pp. 839-857, Terra Sci., Tokyo, 1999.

Freund, F., and R. Ho, Organic matter supplied to a planet by tectonic and volcanic activity, in *Circumstellar Habitable Zones*, edited by L.R. Doyle, pp. 71-98, Travis House, Menlo Park, Calif., 1996.

Freund, F., and M.M. Masuda, Highly mobile oxygen hole-type charge carriers in fused silica, *J. Mater. Res., 8*, 1619-1622, 1991.

Freund, F., and G. Oberheuser, Water dissolved in olivine: A single crystal infrared study, *J. Geophys. Res., 91*, 745-761, 1986.

Freund, F., and H. Wengeler, The infrared spectrum of OH^--compensated defect sites in C-doped MgO and CaO single crystals, *J. Phys. Chem. Solids, 43*, 129-145, 1982.

Freund, F., M.M. Freund, and F. Batllo, Critical review of electrical conductivity measurements and charge distribution analysis of magnesium oxide, *J. Geophys. Res., 98*, 22,209-22,229, 1993.

Freund, F., E.-J. Whang, F. Batllo, L. Desgranges, C. Desgranges, and M.M. Freund, Positive hole-type charge carriers in oxide materials, in *Grain Boundaries and Interfacial Phenomena in Electronic Ceramics*, edited by L.M. Levinson, pp. 263-278, Am. Ceram. Soc., Cincinnati, Ohio, 1994.

Friebele, E.J., D.L. Griscom, M. Stapelbroek, and R.A. Weeks, Fundamental defect centers in glass: The peroxy radical in irradiated high-purity fused silica, *Phys. Rev. Lett., 42*, 1346-1349, 1979.

Fritz, P., and S.K. Frape, Saline Water and Gases in Crystalline Rocks, in Geol. Assoc. Can., *Spec. Pap. 33*, 259 pp., 1987.

Frost, B.R., and K. Bucher, Is water responsible for geophysical anomalies in the deep continental crust?, *Tectonophysics, 231*, 293-309, 1994.

Frost, B.R., W.S. Fyfe, and K. Tazaki, Grain boundary graphite in rocks and implication for high electric conductivity in the lower crust, *Nature, 340*, 134-136, 1989.

Fujinawa, Y. and K. Takahashi, Emission of electromagnetic radiation preceding the Ito seismic swarm of 1989, *Nature, 347*, 376-378, 1990.

Fujinawa, Y., and K. Takahashi, Electromagnetic field changes as a precursory phenomena of earthquakes and volcanic eruptions, report, Nat. Res. Inst. for Earth Sci. and Disaster Prev., Tokyo, 1993.

Galperin, Y.I. et al., VLF and ELF effects in the upper ionospheric caused by large-scaled acoustic waves in the lower ionosphere observed from aurol-3 satellite, in *Result of the ARCAD-3 Project and of the Recent Programmes in Magnetospheric and Ionospheric Physics*, pp. 661-684, *Cent. Natl. d'Etudes Spatiales, Toulouse*, France, 1985.

Geller, R.J., Debate on VAN, *Geophys. Res. Lett., 23* (11), 1291-1452, 1996.

Geller, R.J., Earthquake prediction: a critical review, *Geophys. J. Int., 131*, 425-250, 1997.

Gokhberg, M.B., A.V. Kustov, V.A. Liperovsky, R.K. Liperovskaya, E.P. Kharin, and S.L. Shalimov, On perturbations in the ionospheric F-region prior to strong earthquakes, *Izv. Akad. Nauk SSSR, Fiz. Zemli, N4*, 12-20, 1988.

Griscom, D.L., Electron spin resonance, *Glass· Sci. Technol.*, Amsterdam, *4B*, 151-251, 1990.

Hadjicontis, V., and C. Mavromatou, Transient electric signals prior to rock failure under uniaxial stress, *Geophys. Res. Lett., 21*, 1687-1690, 1994.

Hamann, D.R., Diffusion of atomic oxygen in SiO_2, *Phys. Rev. Lett.*, 16, 3447-3450, 1998.

Hedervari, P., and Z. Noszticzius, Recent results concerning earthquake lights, *Ann. Geophys., 3*, 705-708, 1985.

Horn, R.G., and D.T. Smith, Contact electrification and adhesion between dissimilar materials, *Science, 256*, 362-365, 1992.

Huang, Q., and M. Ikeya, Seismic electromagnetic signals (SEMS) explained by a simulation experiment using electromagnetic waves, *Phys. Earth Planet. Inter., 109*, 107-114, 1998.

Johnston, A.C., Light from seismic waves, *Nature, 354*, 361, 1991.

Johnston, M.J.S., Review of electric and magnetic fields accompanying seismic and volcanic activity, *Surveys in Geophysics, 18*, 441-475, 1997.

Kariya, K.A., and T.J. Shankland, Electrical conductivity of dry lower crustal rocks, *Geophysics*, *48*, 52-61, 1983.

Kathrein, H., and F. Freund, Electrical conductivity of magnesium oxide single crystals below 1200 K., *J. Phys. Chem. Solids*, *44*, 177-186, 1983.

King, B.V., and F. Freund, Surface charges and subsurface space charge distribution in magnesium oxide containing dissolved traces of water., *Phys. Rev.*, *B 29*, 5814-5824, 1984.

Kittel, C., *Introduction to Solid State Physics*, J. Wiley & Sons, New York, 1980.

Kopytenko, Y.A., T. Matiashvili, P.M. Voronov, E.A. Kopytenko, and O.A. Molchanov, Detection of ultra-low-frequency emissions connected with the Spitak earthquake and its aftershock activity, based on geomagnetic pulsation data at Dusheti and Vardzia observatories, *Phys. Earth Planet. Inter.*, *77*, 88-95, 1993.

Larkina, V.I., V.V. Migulin, O.A. Molchanov, A.S. Ilchin, and V.V. Shvetsova, Characteristics of the excitation of low-frequency emissions in the upper ionosphere above earthquake regions, *Geomagn. Aeron.*, *28*, 685-689, 1988.

Marfunin, A. S., *Spectroscopy, Luminescence and Radiation Centers in Minerals*, Springer-Verlag, New York, 1979.

Martens, R., H. Gentsch, and F. Freund, Hydrogen release during the thermal decomposition of magnesium hydroxide to magnesium oxide, *J. Catal.*, *44*, 366-372, 1976.

Masood, E., Greek earthquake stirs controversy over claims for prediction, *Nature*, *375*, 617, 1995.

Merzer, M., and S.L. Klemperer, Modeling low-frequency magnetic-field precursors to the Loma Prieta earthquake with a precursory increase in fault-zone conductivity, *Pure Appl. Geophys.*, *150*, 217-248, 1997.

Meyer, L.L., *California Quake*, Sherbourne, Nashville, Tenn., 1977.

Michael, A.J., Testing prediction methods: Earthquake clustering versus the Poisson model, *Geophys. Res. Lett.*, *24*, 1891-1894, 1996.

Molchanov, O.A., and M. Hayakawa, Subionospheric VLF signal perturbations possibly related to earthquakes, *J. Geophys. Res.*, *103*, 17,489-17,504, 1998a.

Molchanov, O.A., and M. Hayakawa, On the generation mechanism of ULF seismogenic electromagnetic emissions, *Phys. Earth Planet. Inter.*, *105*, 201-210, 1998b.

Molchanov, O.A., Y.A. Kopytenko, E.A. Kopytenko, T. Matiashvili, A.C. Fraser-Smith, and A. Bernardi, Results of ULF magnetic field measurements near the epicenters of the Spitak (M_s=6.9) and Loma Prieta (M_s=7.1) earthquakes: Comparative analysis, *Geophys. Res. Lett.*, *19*, 1495-1498, 1992.

Molchanov, O.A., M. Hayakawa, T. Oudoh, and E. Kawai, Precursory effects in the subionospheric VLF signals for the Kobe earthquake, *Phys. Earth Planet. Inter.*, *105*, 239-248, 1998.

Morat, P., and J.L. LeMouel, Variation of the electric resistivity of large rock samples with stress, *Geophysics*, *52*, 1424-1430, 1987.

Morat, P., and J.-L. LeMouel, Electrical signals generated by stress variations in porous non-saturated rocks, *C. R. Acad. Sci., Ser. II*, *315*, 955-963, 1992.

Morrison, F.D., E.R. Williams, and T.D. Madden, Streaming potentials of Westerly granite with applications, *J. Geophys. Res.*, *94*, 12,449-12,461, 1989.

Nitsan, U., Electromagnetic emission accompanying fracture of quartz-bearing rocks, *Geophys. Res. Lett.*, *4*, 333-336, 1977.

Nur, A., Matsushiro, Japan, earthquake swarm: Confirmation of the dilatancy-fluid diffusion model, *Geology*, *2*, 217-221, 1974.

Oommen, T.V., Static electrification properties of transformer oil, *IEEE Trans. Electr. Insul.*, *23*, 123-128, 1988.

Park, S.K., Electromagnetic precursors to earthquakes: A search for predictors, *Sci. Progr.*, *80*, 65-82, 1997a.

Park, S.K., Monitoring resistivity change in Parkfield, California: 1988-1995, *J. Geophys. Res.*, *102*, 24,545-24,559, 1997b.

Park, S.K., Variation in electrical properties induced by stress along the San Andreas Fault at Parkfield, California, University of California, Riverside, CA, 1998.

Park, S.K., M.J.S. Johnston, T.R. Madden, F.D. Morgan, and H.F. Morrison, Electromagnetic precursors to earthquakes in the ULF band: A review of observations and mechanisms, *Rev. Geophys.*, *31*, 117-132, 1993.

Parrot, M., and M.J.S. Johnston, (Eds.), Seismoelectromagnetic effects, *Phys. Earth Planet. Inter.*, *57*, 1-177, 1989.

Pham, V.N., D. Boyer, G. Chouliaras, J.L. LeMouel, J.C. Rossignol, and G.N. Stavrakakis, Characteristics of electromagnetic noises in Ioannina region (Greece): A possible origin for so called "seismic electric signals" (SES), *Geophys. Res. Lett.*, *25*, 2229-2232, 1998.

Quellet, M., Earthquake light and seismicity, *Nature*, *348*, 492, 1990.

Rikitake, T., *Earthquake Prediction*, Elsevier, New York, 1976.

Rossman, G.R., Studies of OH in nominally anhydrous minerals, *Phys. Chem. Miner.*, *23*, 299-304, 1996.

Schock, R.N., and A. Duba, Point defects and the mechanisms of electrical conduction in olivine, in *Point Defects in Minerals*, Geophys. Monogr. Ser., vol. 31, edited by R.N. Schock, pp. 88-96, Washington, D.C., 1985.

Sempolinski, D.R., and W.D. Kingery, Ionic conductivity and magnesium vacancy mobility in magnesium oxide, *J. Am. Ceram. Soc.*, *63*, 664-669, 1980.

Serebryakova, O.N., S.V. Bilichenko, V.M. Chmyrev, M. Parrot, J.L. Rauch, F. Lefeuvre, and O.A. Pokhotelov, Electromagnetic ELF radiation from earthquake regions as observed by low-altitude satellites, *Geophys. Res. Lett.*, *19*, 91-94, 1992.

Shankland, T.J., Electrical conduction in mantle materials, in *Evolution of the Earth*, Geodyn. Ser., vol. 5, edited by R.J. O'Connell and W.S. Fyfe, pp. 256-263, Washington, D.C., 1981.

Shankland, T.J., and M.E. Ander, Electrical conductivity, temperature and fluids in the crust, *J. Geophys. Res.*, *88*, 9475-9484, 1983.

Shluger, A.L., E.N. Heifets, J.D. Gale, and C.R.A. Catlow, Theoretical simulation of localized holes in MgO, *J. Phys. Condens. Matter*, *4*, 5711-5722, 1992.

Smyth, J.R., D.R. Bell, and G.R. Rossman, Incorporation of hydroxyl in upper-mantle clinopyroxenes, *Nature*, *351*, 732-735, 1991.

Stesky, R.M., Electrical conductivity of brine-saturated fractured rock, *Geophysics*, *51*, 1585-1593, 1986.

Tributsch, H., *When Snakes Awake: Animals and Earthquake Prediction*, MIT Press, Cambridge, Mass., 1983.

Valley, J.W., S.R. Bohlen, E. Essene, and W. Lamb, Metamorphism in the Adirondacks, II, The role of fluids, *J. Petrol.*, *31*, 555-596, 1990.

Varotsos, P., N. Sarlis, M. Lazaridou, and P. Kapiris, Transmission of stress induced electric signals in dielectric media, *J. Appl. Phys.*, *83*, 60-70, 1997.

Wannamaker, P.E., Fluids in the Earth's crust: Electromagnetic constraints on existence and distribution, *U.S. Geol. Surv. Open File Rep.*, *94-228*, 162-177, 1994.

Wannamaker, P.E., Comment on "The petrologic case for a dry lower crust" by B.W.D. Yardley and J.W. Valley, *J. Geophys. Res.*, *105*, 6057-6064, 2000.

Wuensch, B.J., W.C. Steele, and T. Vasilos, Cation self-diffusion in single crystal MgO, *J. Chem. Phys.*, *58*, 5258-5266, 1973.

Yardley, B.W.D., and J.W. Valley, The petrologic case for a dry lower crust, *J. Geophys. Res.*, *102*, 12,173-12,185, 1997.

Yardley, B.W.D., and J.W. Valley, Reply to comment by P.E. Wannamaker on "The petrologic case for a dry lower crust", *J. Geophys. Res.*, *105, 6065-6068, 2000.*

Yoshida, S., M. Nakatani, and T. Asada, Observations of electromagnetic radiation associated with aftershocks of the Hyogoken-nanbu earthquake, *Bull. Earthquake Res. Inst. Univ. Tokyo*, *70*, 1-8, 1995.

Yoshida, S., M. Uyeshima, and M. Nakatani, Electric potential changes associated with slip failure of granite: Preseismic and coseismic signals, *J. Geophys. Res.*, *102*, 14,883-14,897, 1997.

Yoshida, S., O.C. Clint, and P.R. Sammonds, Electric potential changes prior to shear fracture in dry and saturated rocks, *Geophys. Res. Lett.*, *25*, 1577-1580, 1998.

Zhijia, Z., Investigation of tectonomagnetic phenomena in China, *Phys. Earth Planet. Inter.*, *57*, 11-22, 1989.

F. Freund, NASA Ames Research Center, MS 239-15, Moffett Field, CA 94035-1000. (freund@mail.arc.nasa.gov)

(Received June 7, 1999; revised October 4, 1999;
accepted December 1, 1999)